

REPORT DOCUMENTATION PAGE

Form Approved  
OMB No. 0704-0188

Use of reporting burden for this collection of information is estimated to average 1 hour per response, including the time for reviewing instructions, searching existing data sources, gathering and maintaining the data needed, and completing and reviewing the collection of information. Send comments regarding this burden estimate or any aspect of this collection of information, including suggestions for reducing the burden, to Washington Headquarters Services, Directorate for Information Operations and Reports, 1215 Jefferson Davis Highway, Suite 1204, Arlington, VA 22202-4302, and to the Office of Management and Budget, Paperwork Reduction Project (0704-0188), Washington, DC 20503.

1. AGENCY USE ONLY (Leave blank)		2. REPORT DATE DEC 1993	3. REPORT TYPE AND DATES COVERED THESIS/DISSERTATION	
4. TITLE AND SUBTITLE SPIN-UP IN A RECTANGULAR CYLINDER			5. FUNDING NUMBERS <b>AD-A275 465</b>	
6. AUTHOR(S) DAWN L. STEWART				
7. PERFORMING ORGANIZATION NAME(S) AND ADDRESS(ES) AFIT Student Attending: THE PENNSYLVANIA STATE UNIV			8. PERFORMING ORGANIZATION REPORT NUMBER AFIT/CI/CIA- 93-163	
9. SPONSORING/MONITORING AGENCY NAME(S) AND ADDRESS(ES) DEPARTMENT OF THE AIR FORCE AFIT/CI 2950 P STREET WRIGHT-PATTERSON AFB OH 45433-7765			10. SPONSORING/MONITORING AGENCY REPORT NUMBER	
11. SUPPLEMENTARY NOTES				
12a. DISTRIBUTION/AVAILABILITY STATEMENT Approved for Public Release IAW 190-1 Distribution Unlimited MICHAEL M. BRICKER, SMSgt, USAF Chief Administration			12b. DISTRIBUTION CODE	
13. ABSTRACT (Maximum 200 words)  <p style="text-align: center;"><b>DTIC</b> <b>SELECTE</b> <b>FEB 04 1994</b> <b>S B D</b></p>				
14. SUBJECT TERMS			15. NUMBER OF PAGES 58	
			16. PRICE CODE	
17. SECURITY CLASSIFICATION OF REPORT	18. SECURITY CLASSIFICATION OF THIS PAGE	19. SECURITY CLASSIFICATION OF ABSTRACT	20. LIMITATION OF ABSTRACT	

①

93-163

The Pennsylvania State University

The Graduate School

Department of Mathematics

**SPIN- UP IN A RECTANGULAR CYLINDER**

A Thesis in

Mathematics

by

Dawn L. Stewart

Submitted in Partial Fulfillment  
of the Requirements  
for the Degree of

Master of Arts

December 1993

7098 94-03987



94 2 03 201

# DISCLAIMER NOTICE



THIS DOCUMENT IS BEST QUALITY AVAILABLE. THE COPY FURNISHED TO DTIC CONTAINED A SIGNIFICANT NUMBER OF COLOR PAGES WHICH DO NOT REPRODUCE LEGIBLY ON BLACK AND WHITE MICROFICHE.

**The Pennsylvania State University**

**The Graduate School**

**Department of Mathematics**

**SPIN- UP IN A RECTANGULAR CYLINDER**

**A Thesis in**

**Mathematics**

**by**

**Dawn L. Stewart**

**Submitted in Partial Fulfillment  
of the Requirements  
for the Degree of**

**Master of Arts**

**December 1993**

We approve the thesis of Dawn L. Stewart.

Date of Signature

*Diane Henderson*

Diane Henderson  
Assistant Professor of Mathematics  
Thesis Advisor

12 OCT 93

*Juan Lopez*

Juan Lopez  
Associate Professor of Mathematics

12 OCT 1993

*William Pritchard*

William Pritchard  
Professor of Mathematics

12 Oct 93

*Joel Anderson*

Joel Anderson  
Professor of Mathematics  
In Charge of Graduate Programs in Mathematics

OCT 12, 1993

DTIC QUALITY INSPECTED 8

Accession For	
NTIS GRA&I	<input checked="" type="checkbox"/>
DTIC TAB	<input type="checkbox"/>
Unannounced	<input type="checkbox"/>
Justification	
By _____	
Distribution/ _____	
Availability Codes	
Dist.	Avail and/or Special
A-1	

## ABSTRACT

We examined the spin-up from rest of water in a rectangular cylinder. The presence of corners in the cylinder causes the formation of eddies. We found that the number of eddies, as well as eddy size, position, and rotation rate were dependent on the aspect ratio of the cylinder, the depth of the fluid, and the final angular velocity of the cylinder. Two time scales were found to be important in this experiment: the traditional Ekman number based on depth, which defines the time scale required for spin-up and an additional Ekman number based on the cylinder length which provides some information about the evolution of the fluid pathlines in route to spin-up. This second Eckman number appears to provide an explanation for both the agreement and disagreement of the experimental results herein and previously published results.

## Table of Contents

LIST OF FIGURES .....	v
LIST OF TABLES .....	vii
ACKNOWLEDGMENTS .....	viii
Chapter 1. INTRODUCTION .....	1
Chapter 2. LITERATURE REVIEW .....	4
Chapter 3. THEORETICAL CONSIDERATIONS .....	8
3.1 Equations of Motion for Spin-up in a Rectangular Cylinder .....	8
3.2 Streamlines for the Initial Flow .....	10
3.3 Linear Solution for the Circular Cylinder .....	12
Chapter 4. EXPERIMENTAL EQUIPMENT AND PRODECURES .....	17
4.1 Real-Time Computer .....	17
4.2 Turntable and Drive .....	18
4.3 Flow Visualization .....	23
4.4 The Rectangular Tank and Water .....	24
Chapter 5. RESULTS .....	26
5.1 Comparison Case .....	27
5.1.1 Horizontal Flow Observations .....	27
5.1.2 Vertical Flow Observations .....	30
5.1.3 Comparison with vHDD's Experiment .....	32
5.2 Effects of Varying $\delta$ .....	35
5.3 Effects of Varying $H$ .....	39
5.4 Effects of Varying $\Omega_f$ .....	43
5.5 Path of the Eddy Center .....	48
5.6 Path of a Separation Point of the Flow .....	48
5.7 Post Spin-up Phenomena .....	51
Chapter 6. CONCLUSIONS .....	56
BIBLIOGRAPHY .....	58

## LIST OF FIGURES

2.1	Cross-sectional View of the Secondary Flow .....	5
3.1	Schematic View of the Rectangular Cylinder .....	8
3.2	The Stream Function, $\psi$ , in the Rotating Reference Frame at the Onset of Spin-up. ....	11
4.1	Schematic of the Computer, Turntable, and Drive Assembly .....	17
4.2	Motor Calibration Curve .....	18
4.3	Schematic of the Table/Tank Assembly .....	19
4.4	Frequency Spectra of the Perturbative Surface Waves .....	22
4.5	Data Points Showing the Measurement Error for the Position of the Eddy Center .....	25
5.1	Plan View of the Rectangular Cylinder .....	26
5.2	Photographs of Dyelines for Spin-up from Rest .....	29
5.2.1	Approximate Trace for the Observed Vertical Flow Patterns in the Eddies .....	31
5.3	Photographs of Dyelines as a Function of $\delta$ ..	37
5.4	The Angle of the 3-Cell Axis as a Function of Aspect Ratio. ....	40
5.5	Photographs of Dyelines as a Function of H .....	41
5.6	Photographs of Dyelines as a Function of $\Omega_f$ .....	45
5.7	Path of the Center of the Cyclonic Eddy. ....	49
5.8	Distance from the Cylinder's Corner to the Center of the Cyclonic Eddy as a Function of Time .....	50
5.9	Path of a Separation Point of the Flow along the x-endwall. ....	51
5.10	Surface Waves Evidenced in the Dyelines after Spin-up .....	52

5.11 Post Spin-up Dyeline Instability ..... 52

5.12 Post Spin-up Vortex Development ..... 54

5.13 Post Spin-up Vortex Development ..... 55

## LIST OF TABLES

5.1	Characteristic Parameters and Non-dimensional Numbers for One of vHDD's Experiments and Two Experiments Herein .....	33
-----	---	----

## ACKNOWLEDGMENTS

I wish to thank my advisor, Dr Diane Henderson, whose dedication to experimental fluid mechanics and insightful guidance provided the motivation for performing this research. Her enduring patience and encouragement gave me the strength to see it through in the face of ever-conflicting priorities.

Thanks also to my other committee members, Dr William Pritchard and Dr Juan Lopez, for their valuable comments regarding this thesis.

I would also like to extend my appreciation to Mr Robert Geist whose tireless support in the lab was an essential and valuable contribution to this thesis.

Many thanks to my family whose love and understanding is a never-ending source of inspiration.

Finally, I would like to thank the USAF for sponsoring my master's program. The equipment for this research was funded by Penn State and grants from the David and Lucille Packard, and Keck Foundations.

## Chapter 1

### INTRODUCTION

Spin-up is the flow of a contained fluid that changes from one state of rigid body rotation to another when the container's rotation rate is increased from a steady, initial angular speed of  $\Omega_0$  to a steady, final angular speed of  $\Omega_f$ . Applications of spin-up include motions in the Earth's core, the stability of liquid-filled projectiles, the transient development of wind-driven coastal upwellings, and the interior rotation of the sun (Benton and Clark, 1974). Spin-up is also encountered in models of global ocean circulation that are started from rest and attempt to develop a quasi-steady circulation pattern (Pond & Pickard, 1983, p183-190). These problems all involve nonlinear systems whose multi-parameters are difficult to identify and isolate. Herein, we consider a seemingly simple system that is in fact somewhat complicated - the spin-up from rest of water in a right, rectangular cylinder. The flow depends on a number of parameters including water depth,  $H$ , horizontal aspect ratio,  $\delta$ , and  $\Omega_f$ . We describe an experimental investigation of the effects of varying these parameters on the evolution of the flow during spin-up and the pathlines of the flow at spin-up.

Despite the complications that are specific to any given system undergoing spin-up, some of the basic physics is similar. In particular, the flow involves viscous boundary layers at the walls and an inviscid flow in the interior. The prototype system for study is the spin-up of water in a right circular cylinder. As the angular velocity of the cylinder is increased from  $\Omega_0$  to  $\Omega_f$ , the interior fluid is unaffected with pressure gradient forces balancing centrifugal forces. However, because of the no-slip boundary condition, the fluid on the boundaries has the angular speed of the cylinder. The resulting large viscous stresses rapidly cause the fluid near the cylinder boundaries to accelerate. In the absence of horizontal boundaries, the angu-

lar velocity at the sidewall diffuses into the interior due to viscosity. The presence of horizontal boundaries, though, creates a different phenomenon. As the angular velocity of the fluid in the horizontal boundary layers increases, the centrifugal force soon overcomes the prevailing pressure gradient force, causing the fluid to be thrown radially outward. Conservation of mass requires that the fluid thrown outward be replaced by fluid from the inviscid interior and a much slower, secondary flow is established. This secondary flow is the key to the spin-up process. The secondary flow convects high angular momentum fluid away from the cylinder sidewalls toward the rotation axis. As the fluid moves into the interior, its angular momentum is conserved. Thus the secondary flow transports higher angular-momentum fluid into the cylinder interior faster than would occur if viscous diffusion was the only process involved. Once the fluid is rotating uniformly at the new angular velocity,  $\Omega_f$ , we say it is spun-up.

The physics described above applies to spin-up in the rectangular cylinder in a general sense; however, the presence of corners causes flow separation that results in the formation of eddies that evolve within the interior of the flow. Numerous and varied eddy configurations result from the spinning-up of fluid in a rectangular cylinder. Let  $n$  be the integer value nearest to the value of the horizontal aspect ratio,  $\delta$ . In general, we have found that if  $n$  is odd, then the pathlines of the flow at spin up form  $\delta$  circular cells, which are antisymmetric about the diagonals of the cylinder and have vorticity (before spin-up) at the narrow walls that has the sense of the cylinder's rotation. This result is in contrast with that of van Heijst, Davies, and Davis (1990), hereafter vHDD, who observed that the vorticity (before spin-up) at the narrow walls has the opposite sense of the cylinder's rotation. If  $n$  is even, the flow evolves into an odd number of cyclonic and anti-cyclonic cells whose centers are not on a common horizontal axis. This result is true when the change in rotation rate,  $\Delta\Omega$ , is relatively

small and the water is relatively deep. However, as we increase  $\Delta\Omega$ , or decrease the water depth,  $H$ , the flow patterns change. For example, our results mimic those of vHDD in experiments for which an Ekman number based on the (long) length of the cylinder is small enough. In Chapter 5, we describe the results of changing  $\delta$ ,  $H$ , and  $\Omega_f$ .

A more thorough review of previous research concerning spin-up will be presented in Chapter 2. Chapter 3 describes the basic equations governing the flows and a linear solution for spin-up in a circular cylinder. The experimental equipment and procedures are discussed in Chapter 4, and the results are presented in Chapter 5.

## Chapter 2

### Literature Review

Previous research on spin-up has consisted primarily of theoretical and experimental studies of spin-up in axisymmetric cylinders. We briefly review this work to discuss the basic physics of fluid undergoing spin-up. (See Greenspan (1968) and Benton & Clark (1974) for comprehensive reviews.) We then discuss previous work on spin-up in non-axisymmetric cylinders.

The first linear model describing the spin-up of a homogeneous fluid in a closed axisymmetric container was provided by Greenspan and Howard (1963). They examined the limiting case of an infinite circular cylinder of radius  $A$ . In this case, they found that the mechanism for spin-up is the diffusion of vorticity that arises at the lateral boundaries. Rigid body rotation is achieved in a dimensional time of order  $T_v = A^2/\nu$ , where  $\nu$  is the kinematic viscosity of the fluid. Next, they analyzed the opposite extreme, that of two parallel coaxial infinite disks separated by a distance of  $2H$ . In this case, they found that the spin-up consisted "of three distinct phases: the development of the Ekman layer, the inviscid fluid spin-up, and the viscous decay of residual oscillations." They determined that the dimensional spin-up time, which Greenspan and Howard defined as the time required for the interior flow to approach the final state of rigid rotation within  $e^{-1}$ , is of order  $T_E = (H^2/\nu\Omega)^{1/2}$ . Using these results for two parallel coaxial infinite disks, they used a perturbation expansion in half-powers of  $E$  to study the case of an arbitrary axisymmetric closed container. Greenspan and Howard noted that if the container has a vertical sidewall a viscous boundary layer, with a double structure different from that Ekman boundary layer, is formed. These layers affect only a small portion of the fluid near the sidewall prior to spin-up. Thus, the spin-up time

scale is still of order  $T_E$  unless the container is elongated in the vertical direction to the extent that the ratio  $H/L$  (depth/width)  $\geq E^{-1/4}$  in which case the time scale for spin-up is again the viscous time-scale,  $T_v$ . Greenspan and Howard also discuss the two effects of having a free surface. First, the Ekman layer at the top boundary is removed so the secondary flow changes from a 4-cell circulation to a 2-cell circulation (See Figure 2.1). Second, they note that the pressure gradient that arises from the parabolic shape of the free surface induces a radial motion toward the interior in addition to the secondary flow produced by the Ekman layer on the bottom of the cylinder. This radial motion acts to decrease the spin-up time. The Froude number,  $F = \Omega^2 L^2 / gH$ , where  $\Omega L$  is the characteristic velocity, is a measure of the relative importance of this free-surface effect.

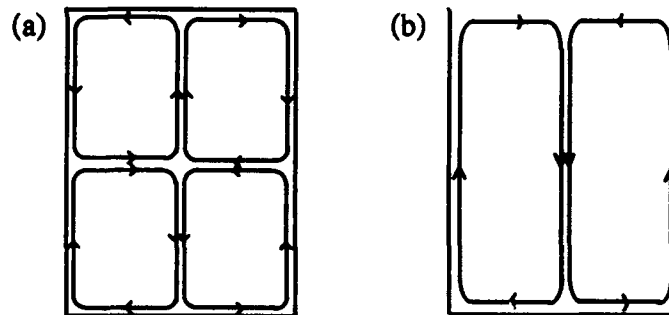


Figure 2.1 Cross-sectional View of the Secondary Flow. (a) rigid lid (b) free surface.

The first non-linear model of the spin-up of a homogeneous fluid within a circular cylinder of finite length and radius was done by Wedemeyer (1964). He divided the flow into two distinct regions, the boundary layer flow near the end walls of the cylinder and the core flow. He derived a nonlinear, inhomogeneous hyperbolic partial differential equation for the radial component of the core flow. The solution to the equation showed that the core

flow is divided into two regions: an inner region in which the fluid particles do not rotate, and an outer region in which the particles spin-up. The regions are separated by a cylindrical front of fluid which moves toward the axis of rotation.

Weidman (1976) did extensive experimental work to examine the theoretical work of Wedemeyer (1964). Weidman noted that one result of the Wedemeyer theory is an  $O(1)$  velocity discontinuity that arises in the inviscid Wedemeyer model when the full nonlinear Ekman suction is included in the spin-up equations. Weidman's measurements of the azimuthal velocity for spin-up in a circular cylinder indicated that this velocity discontinuity is smoothed out in a shear layer whose thickness is a function of radius and time and scales with  $E^{1/4}H$ . He noted that the velocity distributions changed depending on whether the ratio of the wall acceleration period,  $T_a = |(\Omega_i - \Omega_f)/\alpha|$ , where  $\alpha$  is the cylinder acceleration rate, to the ordinary Ekman spin-up time,  $T_E$ , was less than or greater than  $O(1)$ . Weidman observed that for small accelerations,  $T_a/T_E > O(1)$ , measured velocities agreed well with the Wedemeyer theory away from the propagating shear layer. The effect of the shear layer is local and does not affect the large scale flow. At large accelerations,  $T_a/T_E < O(1)$ , Weidman found significant deviations between the experiments and Wedemeyer's theory. In this case, the effect of the shear layer was not negligible.

As noted before, the models described above were all for axisymmetric geometries. A study of spin-up phenomena in non-axisymmetric cylinders was done by van Heijst (1989). He presented experimental observations of spin-up for several geometries: (i) an annular region between two coaxial cylinders with a radial barrier between the cylinder walls; (ii) a semicircle region; (iii) a circular region with a radial barrier extending from the center to the tank wall; and (iv) a region enclosed by two non-concentric cylinders connected by a radial barrier. vHDD (1990) studied spin-up in a rectangular container. In each

of these experiments, the authors observed three main stages in the spin-up process: (i) the starting flow, characterized by zero absolute vorticity, (ii) flow separation, and (iii) a subsequent organization of the flow into an array of alternately cyclonic and anticyclonic circular cells. In the latter experiments, vHDD noted that the central cell in the free-surface experiments was always cyclonic.

## Chapter 3

### THEORETICAL CONSIDERATIONS

In this chapter, we present the equations of motion associated with the rectangular cylinder as well as the boundary and initial conditions associated with the problem of spin-up. We then describe a solution for the flow at some small time increment,  $t = \epsilon$ . Lastly, we review the linear solution for spin-up in a circular cylinder.

#### 3.1 Equations of Motion for Spin-up in a Rectangular Cylinder

Consider a fluid of depth  $H$  in a rectangular cylinder rotating at  $-\Omega\hat{k}$ , with period  $T = 2\pi/\Omega_f$ . In the following analysis, we use a rectangular coordinate system  $(x, y, z)$  that is rotating with the cylinder. The origin is at the water surface in the center of the cylinder as shown in Figure 3.1.

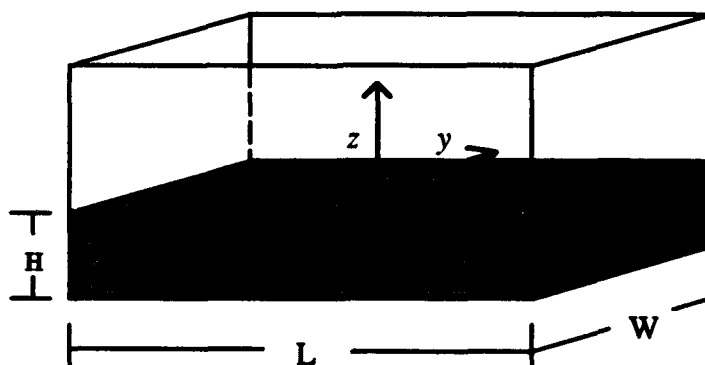


Figure 3.1 Schematic View of the Rectangular Cylinder

The Navier-Stokes equations for a flow with velocity vector  $\mathbf{u}^* = (u^*, v^*, w^*)$  are (the  $*$  denotes dimensional values):

$$\nabla^* \cdot \mathbf{u}^* = 0 \quad 3.1$$

$$\frac{Du^*}{Dt^*} - 2\Omega\hat{k} \times u^* = -\frac{1}{\rho^*}\nabla^* p^* - g\hat{k} + \nu\nabla^{*2}u^* \quad 3.2$$

The boundary conditions are  $u^* = 0$  at  $x^* = \pm \frac{1}{2}L$ ;  $v^* = 0$  at  $y^* = \pm \frac{1}{2}W$ ; and  $w^* = 0$  at  $z^* = 0$ , and  $z^* = -H$  (where, for simplicity, we consider the free surface to behave as a rigid lid).

The pressure,  $p^*$ , consists of perturbations  $\hat{p}^*$  from the hydrostatic pressure.

$$p^* = -\rho^*g^*z^* + \hat{p}^*(x, y, z, t) \quad 3.3$$

To non-dimensionalize the above equations, we scale the  $x$ ,  $y$ , and  $z$  directions by their lengths,  $L$ ,  $W$ , and  $H$  respectively, and time by the final rotation rate  $\Omega_f$ . Since we are interested in an unsteady flow due to a change in rotation speed,  $\Delta$ , we scale velocities by the appropriate length scale times  $\Delta$ . Thus, we have:

$$x = \frac{x^*}{L}; \quad y = \frac{y^*}{W}; \quad z = \frac{z^*}{H} \quad u = \frac{u^*}{L\Delta}; \quad v = \frac{v^*}{W\Delta}; \quad w = \frac{w^*}{H\Delta} \quad 3.4$$

$$t = t^*\Omega_f \quad p = \frac{p^*}{\rho\Omega_f H^2 \Delta} \quad 3.5$$

Then the appropriate non-dimensional numbers are the Ekman number,  $E \equiv \nu/\Omega_f H^2$ , the Rossby number,  $\varepsilon \equiv \Delta/\Omega_f$ , and aspect ratios,  $\alpha$ ,  $\beta$ , and  $\delta$  defined as  $(H/L)^2$ ,  $(H/W)^2$ , and  $L/W$  respectively. So the incompressible Navier-Stokes equations in dimensionless, coordinate form are:

$$\frac{\partial u}{\partial x} + \frac{\partial v}{\partial y} + \frac{\partial w}{\partial z} = 0 \quad 3.6$$

$$\frac{\partial u}{\partial t} + \varepsilon\{u\frac{\partial u}{\partial x} + v\frac{\partial u}{\partial y} + w\frac{\partial u}{\partial z}\} - \frac{2v}{\delta} = -\alpha\frac{\partial \hat{p}}{\partial x} + E\{\alpha\frac{\partial^2 u}{\partial x^2} + \beta\frac{\partial^2 u}{\partial y^2} + \frac{\partial^2 u}{\partial z^2}\} \quad 3.7a$$

$$\frac{\partial v}{\partial t} + \varepsilon\{u\frac{\partial v}{\partial x} + v\frac{\partial v}{\partial y} + w\frac{\partial v}{\partial z}\} - 2\delta u = -\beta\frac{\partial \hat{p}}{\partial y} + E\{\alpha\frac{\partial^2 v}{\partial x^2} + \beta\frac{\partial^2 v}{\partial y^2} + \frac{\partial^2 v}{\partial z^2}\} \quad 3.7b$$

$$\frac{\partial w}{\partial t} + \varepsilon \left\{ u \frac{\partial w}{\partial x} + v \frac{\partial w}{\partial y} + w \frac{\partial w}{\partial z} \right\} = - \frac{\partial \hat{p}}{\partial z} + E \left\{ \frac{\partial^2 w}{\partial x^2} + \frac{\partial^2 w}{\partial y^2} + \frac{\partial^2 w}{\partial z^2} \right\} \quad 3.7c$$

The boundary conditions are  $u = v = w = 0$  at  $x = \pm \frac{1}{2}$ ;  $y = \pm \frac{1}{2}$ ; and  $z = -1$ .

### 3.1 Streamlines for the Initial Flow

If we define a stream function as

$$u = -\psi_y, \text{ and } v = \psi_x \quad 3.9$$

then the vorticity,  $\omega$ , is  $\nabla^2 \psi$ . At the onset of spin-up, the inner flow is quiescent relative to the inertial reference frame, while the flow on the boundaries rotates with the boundaries. In the rotating frame, the sign of the vorticity in the interior is opposite that of the cylinder's rotation (i.e., anticyclonic) and is zero on the boundaries; therefore,  $\nabla^2 \psi = 2$  with  $\psi = 0$  on the boundaries. Hence, a boundary value problem at the onset of spin-up is (following vHDD)

$$\begin{aligned} \nabla^2 \psi &= 2 & \psi &= 0 \text{ at } x = -\frac{1}{2}, \frac{1}{2}; \quad -\frac{1}{2} \leq y \leq \frac{1}{2} \\ & & \psi &= 0 \text{ at } y = -\frac{1}{2}, \frac{1}{2}; \quad -\frac{1}{2} \leq x \leq \frac{1}{2} \end{aligned} \quad 3.10$$

A particular solution of (3.10) is  $\psi_p = (y + 1/2)^2 - (y + 1/2) = y^2 - 1/4$ ; then (3.10) can be transformed into the following homogeneous form of Laplace's equation:

$$\begin{aligned} \nabla^2 \psi_h &= 0 & \psi &= 1/4 - y^2 \text{ at } x = -\frac{1}{2}, \frac{1}{2}; \quad -\frac{1}{2} \leq y \leq \frac{1}{2} \\ & & \psi &= 0 \text{ at } y = -\frac{1}{2}, \frac{1}{2}; \quad -\frac{1}{2} \leq x \leq \frac{1}{2} \end{aligned} \quad 3.11$$

The solution to (3.11) is found using separation of variables and fourier series to be:

$$\psi(x, y) = \frac{8}{\pi^3} \sum_{n=0}^{\infty} \frac{\sin(2n+1)\pi(y + \frac{1}{2})}{(2n+1)^3} \left[ \frac{\sinh(2n+1)\pi(\frac{1}{2} - x)\delta + \sinh(2n+1)\pi(x + \frac{1}{2})\delta}{\sinh(2n+1)\pi\delta} \right] + y^2 - \frac{1}{4} \quad 3.12$$

A plot of  $\psi$  and its contours is shown in Figure 3.1. vHDD observed that experimental streamlines agreed well with the theoretical results described above for  $t/T = .08$  after the onset of spin-up.

### 3.3 Linear Solution for Spin-up in a Circular Cylinder

It is useful to review the linear solution for spin-up in a circular cylinder provided by Greenspan and Howard (1963) in order to understand the mechanism for spin-up and the differences between spin-up in a circular cylinder and spin-up in a rectangular cylinder. Consider a fluid in a circular cylinder of radius,  $A$ , and depth  $H$ , rotating in rigid body rotation about its center with constant angular velocity  $\Omega_i$ . Consider a cylindrical coordinate system  $(r, \theta, z)$  rotating with the cylinder whose origin is in the center of the cylinder. For simplicity, we consider the fluid to have a rigid lid. We seek a solution for the azimuthal velocity in the interior of the cylinder.

The dimensional Navier-Stokes equations for this axially symmetric flow with velocity vector,  $\mathbf{u}^* = (u^*, v^*, w^*)$ , and perturbation pressure,  $\hat{p}^*$ , are:

$$\frac{1}{r^*} \frac{\partial(r^* u^*)}{\partial r^*} + \frac{\partial w^*}{\partial z^*} = 0 \quad 3.13$$

$$\frac{D u^*}{D t^*} - \frac{v^{*2}}{r^*} - 2\Omega v^* = -\frac{1}{\rho} \frac{\partial \hat{p}^*}{\partial r^*} + \nu(\Delta^* u^* - \frac{u^*}{r^{*2}}) \quad 3.14a$$

$$\frac{D v^*}{D t^*} + \frac{u^* v^*}{r^*} + 2\Omega u^* = \nu(\Delta^* v^* - \frac{v^*}{r^{*2}}) \quad 3.14b$$

$$\frac{D w^*}{D t^*} = -\frac{1}{\rho} \frac{\partial \hat{p}^*}{\partial z^*} + \nu \Delta^* w^* \quad 3.14c$$

If we suppose the angular velocity is impulsively increased by a small amount,  $\epsilon \Omega_i$ , then the boundary and initial conditions are  $\mathbf{u}^* = \epsilon \Omega \hat{\mathbf{k}} \times \mathbf{r}$  on the solid boundaries, and  $\mathbf{u}^* =$

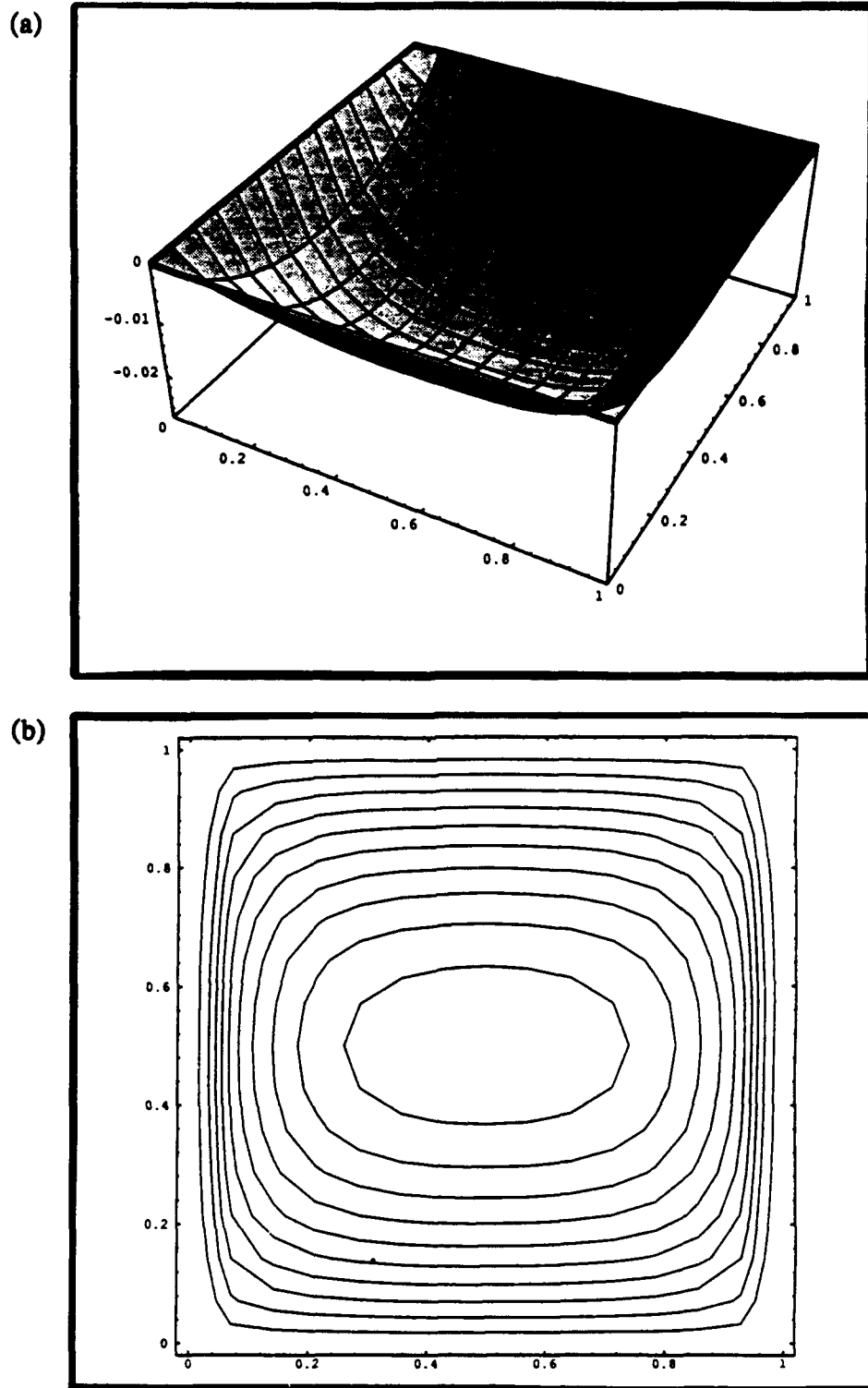


Figure 3.1 The Stream Function,  $\psi$ , in the Rotating Reference Frame at the Onset of Spin-up. (a) surface (b) contours.

0 for  $t \leq 0$ . To non-dimensionalize the above equations, we introduce the following non-dimensional variables

$$r = \frac{r^*}{H}, \quad z = \frac{z^*}{H}, \quad t = t^* \Omega, \quad u = \frac{u^*}{H \epsilon \Omega}, \quad 3.15$$

$$p = \frac{\hat{p}^*}{\rho \epsilon \Omega H^2}, \quad \text{and } E = \frac{\nu}{\Omega H^2}, \quad 3.16$$

where  $\epsilon = (\Omega_f - \Omega_i)/\Omega_i$  is the Rossby number and  $E$  is the Ekman number. Considering the case of  $\epsilon \ll 1$ , we can neglect the nonlinear terms. The linear initial-boundary value problem becomes

$$\frac{1}{r} \frac{\partial(ru)}{\partial r} + \frac{\partial w}{\partial z} = 0 \quad 3.17$$

$$\frac{\partial u}{\partial t} - 2v = -\frac{\partial p}{\partial r} + E(\Delta u - \frac{u}{r^2}) \quad 3.14a$$

$$\frac{\partial v}{\partial t} + 2u = E(\Delta v - \frac{v}{r^2}) \quad 3.14b$$

$$\frac{\partial w}{\partial t} = -\frac{\partial p}{\partial r} + E \Delta w \quad 3.14c$$

with initial condition  $u = 0$  for  $t \leq 0$  and boundary condition  $u = \hat{k} \times r$  on all solid boundaries.

Define a stream function,  $\psi$ , such that

$$u = -\frac{1}{r} \psi_z, \quad \text{and } w = \frac{1}{r} \psi_r, \quad 3.19$$

where the subscripts indicate partial differentiation. The coordinate equations for (3.18) in the case of an axisymmetric cylinder become

$$-\frac{1}{r} \psi_z - 2v = -p_r + E(\Delta(-\frac{1}{r} \psi_z) + \frac{\psi_z}{r^3}), \quad 3.20a$$

$$v_t - \frac{2}{r} \psi_z = +E(\Delta v - \frac{v}{r^2}), \quad 3.20b$$

$$\text{and } \frac{1}{r}\psi_{rr} = -p_z + E\Delta\left(\frac{1}{r}\psi_r\right). \quad 3.20c$$

Rearranging (3.20b) and eliminating  $p$  from (3.20a and c) provides

$$E\left(\Delta v - \frac{v}{r^2}\right) - v_t + \frac{2}{r}\psi_z = 0, \text{ and} \quad 3.21a$$

$$E\left(\Delta\left(-\frac{1}{r}\psi_{zz} - \left(\frac{1}{r}\psi_r\right)_r\right) + \frac{\psi_{zz}}{r^3}\right) + \frac{1}{r}(\psi_{rr} - \frac{1}{r}\psi_r + \psi_{zz})_t + 2v_z = 0. \quad 3.21b$$

The initial condition is  $\psi = v = 0$  for  $t \leq 0$ , and the boundary condition is  $\psi = \frac{\partial\psi}{\partial n} = 0$ , and  $v = r$  on the lateral boundary.

Since the time scale of interest for the infinite parallel disks was shown to be order  $E^{-1/2}\Omega$ , we begin our analysis of the circular cylinder by scaling as follows:

$$\tau = E^{1/2}t, \text{ and } \psi = E^{1/2}\chi, \quad 3.22$$

where we have scaled the radial and vertical flow to be higher order in Ekman number than the azimuthal flow which is  $O(1)$ . Substituting  $\tau$  and  $\chi$  into equations (3.21) we obtain

$$E^{3/2}\left(\Delta v - \frac{v}{r^2}\right) - v_\tau + \frac{2}{r}\chi_z = 0, \text{ and} \quad 3.23a$$

$$E^{3/2}\left(\Delta\left(-\frac{1}{r}\chi_{zz} - \left(\frac{1}{r}\chi_r\right)_r\right) + \frac{\chi_{zz}}{r^3}\right) + \frac{E}{r}(\chi_{rr} - \frac{1}{r}\chi_r + \chi_{zz})_\tau + 2v_z = 0. \quad 3.23b$$

The flow can be divided into an interior and boundary layer flow such that

$$v = v^I + v^B, \text{ and } \chi = \chi^I + \chi^B. \quad 3.24$$

The equations (3.23) for the interior flow to  $O(E^0)$  become

$$v_\tau^I - \frac{2}{r}\chi_z^I = 0, \text{ and} \quad 3.25a$$

$$v_z^I = 0. \quad 3.25b$$

Thus,

$$v^I = v^I(r, \tau), \text{ and} \quad 3.26a$$

$$\chi^I = \frac{zr}{2} v_\tau^I + \chi_0^I(r, \tau). \quad 3.26b$$

This defines the interior flow in terms of (as yet) undetermined functions,  $v^I$  and  $\chi_0^I$ , of  $r$  and  $\tau$ .

In the boundary layer, we introduce a stretched vertical coordinate,  $\zeta$ , such that

$$z = -\frac{1}{2} + E^{1/2}\zeta \quad \text{in the lower boundary layer, and} \quad 3.27a$$

$$z = \frac{1}{2} - E^{1/2}\zeta \quad \text{in the upper boundary layer.} \quad 3.27b$$

Then to  $O(E^0)$  the boundary layer equations are

$$\text{Lower} \quad v_{\zeta\zeta}^B + \frac{2}{r}\chi_\zeta^B = 0, \quad \text{and} \quad \frac{1}{r}\chi_{\zeta\zeta\zeta\zeta}^B - 2v_\zeta^B = 0; \quad 3.28a$$

$$\text{Upper} \quad v_{\zeta\zeta}^B - \frac{2}{r}\chi_\zeta^B = 0, \quad \text{and} \quad \frac{1}{r}\chi_{\zeta\zeta\zeta\zeta}^B + 2v_\zeta^B = 0; \quad 3.28b$$

The boundary conditions for  $\zeta \rightarrow \infty$  are  $v^B = \chi^B = 0$ ; for  $\zeta = 0$ , they are  $v^B + v^I = r$ ,  $\chi^B + \chi^I = 0$ , and  $\frac{\partial \chi^B}{\partial \zeta} = O(E^{1/2})$ .

Taking first integrals of (3.28a), we have

$$v_\zeta^B + \frac{2}{r}\chi^B = f(r, \tau), \quad \text{and} \quad \frac{1}{r}\chi_{\zeta\zeta\zeta}^B - 2v^B = g(r, \tau); \quad 3.29$$

where  $f$  and  $g$  are equivalent to constants of integration. Eliminating  $\chi^B$  from (3.29) gives

$$v_{\zeta\zeta\zeta\zeta}^B + 4v^B = 0. \quad 3.30$$

The boundary conditions,  $v^B(\infty) = 0$ ,  $v^B(0) = r - v^I$ , and  $v_{\zeta\zeta}^B|_0 = 0$ , imply that

$$v^B = (r - v^I(r, \tau))e^{-\zeta} \cos \zeta. \quad 3.31$$

A similar analysis shows that the same formula applies on the upper boundary. From (3.28)

$$\chi^B(0) = \frac{1}{2}r(r - v^J) \text{ on } z = -\frac{1}{2}, \text{ and} \quad 3.32a$$

$$\chi^B(0) = -\frac{1}{2}r(r - v^J) \text{ on } z = \frac{1}{2}. \quad 3.32b$$

The boundary condition,  $\chi^B + \chi^I = 0$ , (3.32), and (3.26b) imply

$$\frac{r}{4}v_\tau^J(r, \tau) - \chi_0^I(r, \tau) = \frac{r}{2}(r - v^J), \text{ and} \quad 3.33a$$

$$\frac{r}{4}v_\tau^I(r, \tau) + \chi_0^I(r, \tau) = \frac{r}{2}(r - u_\theta^I). \quad 3.33b$$

Adding (3.33a and b), we get

$$v_\tau^J(r, \tau) = 2(r - v^J). \quad 3.34$$

Thus, the interior azimuthal flow is

$$v^J(r, \tau) = r(1 - e^{-2\tau}). \quad 3.35$$

or

$$v^J(r, t) = r(1 - e^{-2E^2 t}). \quad 3.36$$

From this result, we see that the interior azimuthal flow is linearly dependent on  $r$  and the spin-up time scale is of order  $T_E = (H^2/\nu\Omega)^{1/2}$ .

## Chapter 4

### Experimental Equipment and Procedures

The experiments were conducted in the Department of Mathematics Fluid Mechanics laboratory. The laboratory equipment consists of a real-time computer, the turntable and drive, two flow visualization systems, and the rectangular tank with prepared water. Figure 4.1 is a schematic of this system, which we describe below.

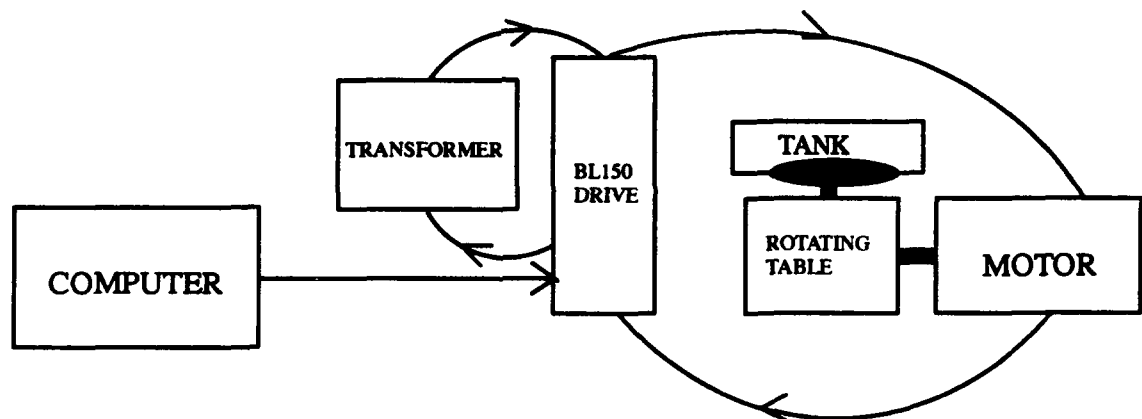


Figure 4.1 Schematic of the Computer, Turntable, and Drive Assembly

#### 4.1 Real-Time Computer

The command signal to the motor drive was from a Digital Equipment Corporation MicroVAX Workstation II with analog-to-digital, and digital-to-analog capabilities, as well as two real-time clocks. In order to minimize transients, we wrote a program to ramp the voltage smoothly from a user-specified initial voltage to the desired final voltage. The program allows the user to input the slope of the ramp (i.e., the time to reach the final volt-

age). For the experiments described herein, we used a 1 sec ramp, sending 1000 incremental voltages to the controller at 1000Hz. The final voltage was then sent to the controller at 500Hz for as long as desired. To determine the relationship between voltage and the rotation rate,  $\Omega$ , of the table, we measured the time for 5 rotations of the table at 12 different voltages. The calibration curve is shown in Figure 4.2. The curve is approximately linear on a log-log scale. Our operating window is between 0 and 8 volts, corresponding to rotation rates,  $\Omega$ , from 0 to 2.1 rad/s.

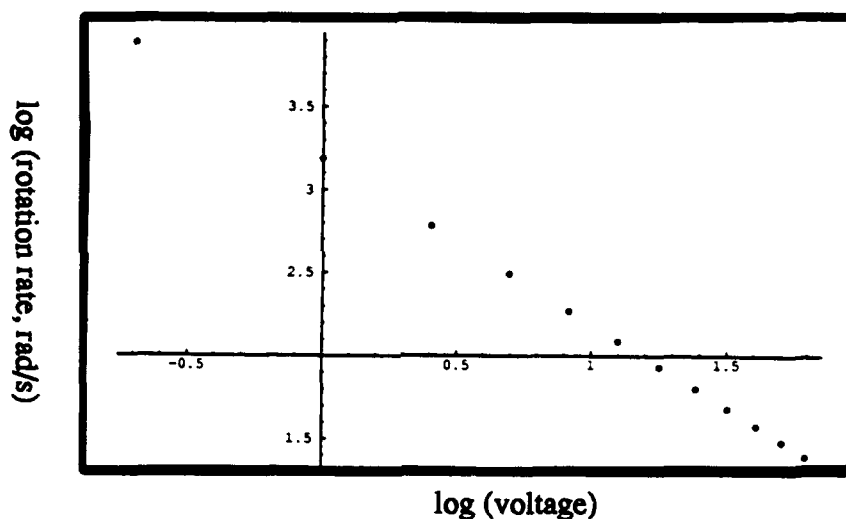


Figure 4.2 Motor Calibration Curve

#### 4.2 Turntable and Drive

The rotating table is a Lintech model MR-308180. The platform is 8 inches in diameter and is mounted to the table shaft with 4 screws located  $11/16$  inches from the center of the table (see Figure 4.3). A large square piece of white lucite,  $13 \frac{1}{3}$  inches on a side, is mounted on the platform using 2 screws located 3 inches from the center of the table. The

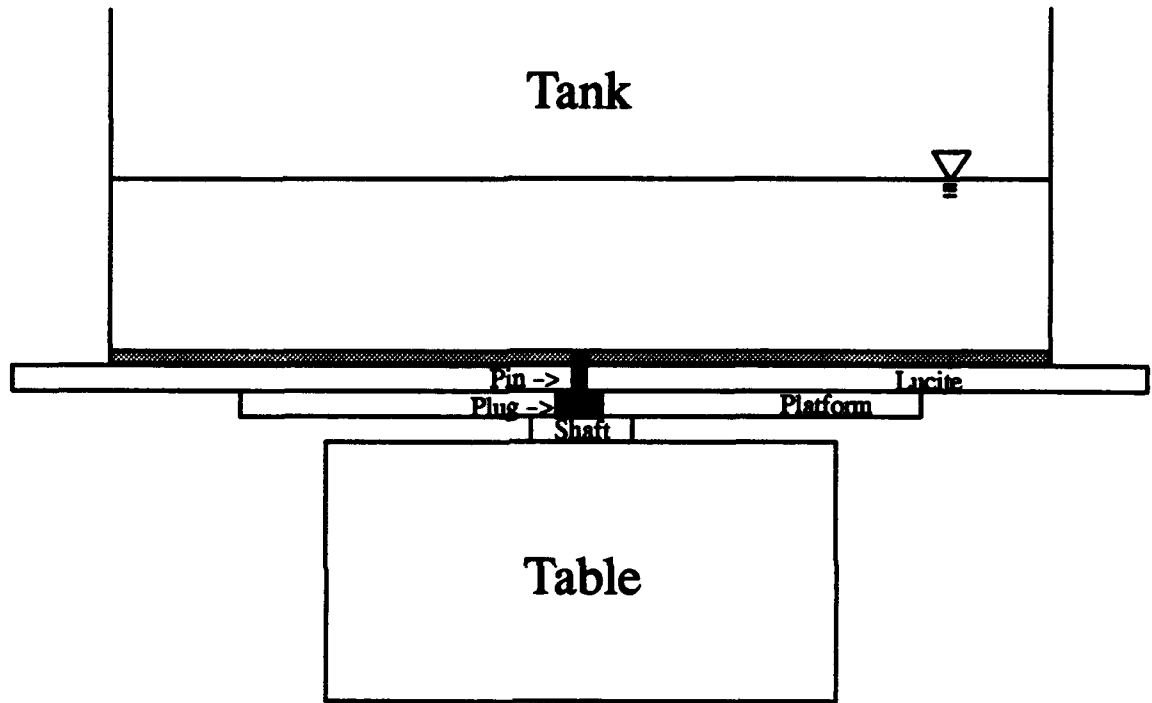


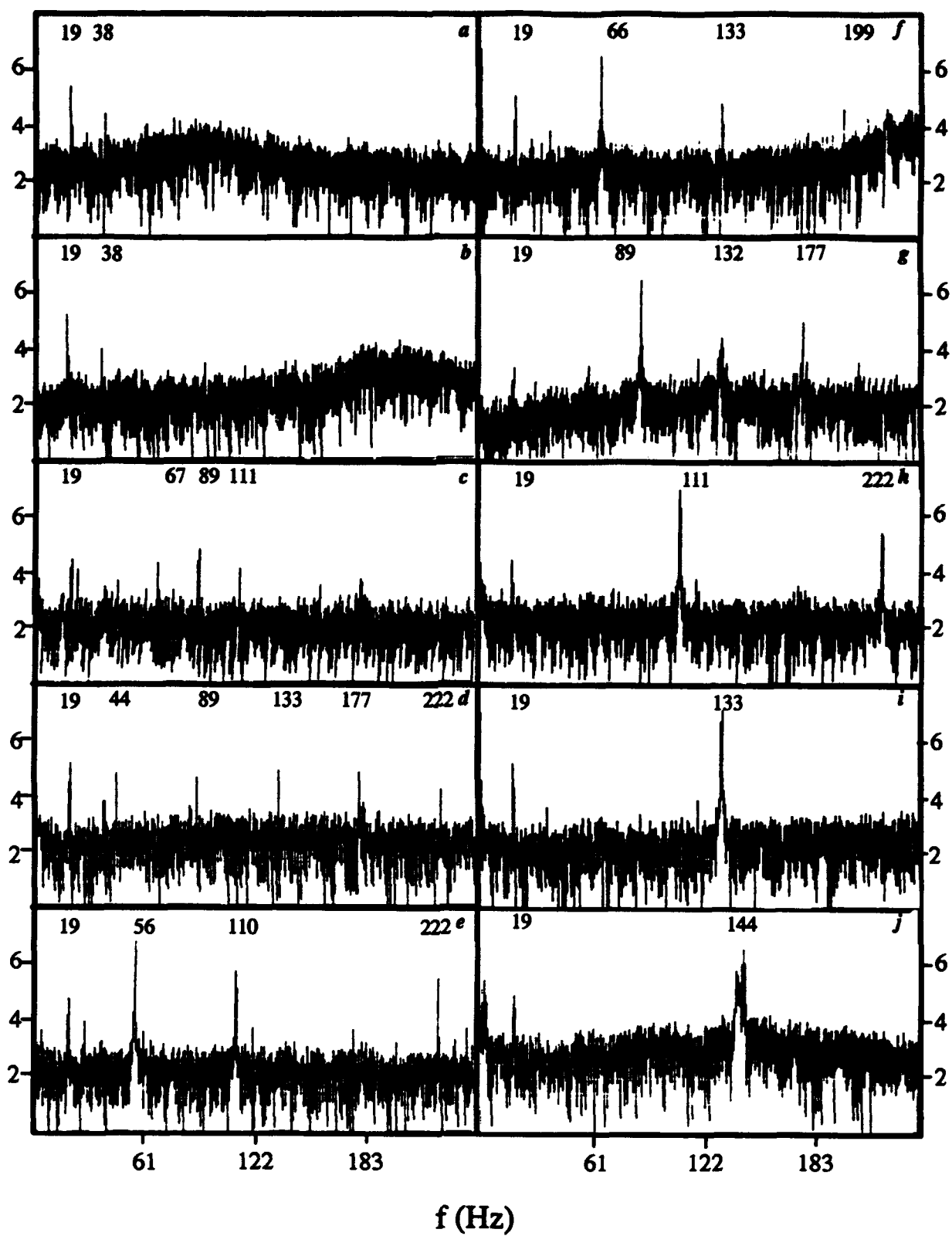
Figure 4.3 Schematic of the Table/Tank Assembly

rectangular cylinder is set on the table using a pin and bracket system, which centers the cylinder to within  $1/500''$ . The pin has a plug on one end that sits in the center of the table; the other end fits tightly into a hole on the bottom of the tank. Four metal brackets hold the container in place. Measurements with a Brown and Taylor dial indicator show that the table itself rotates about its center with an accuracy of  $1/500''$ . The table is level to within  $5.8 \times 10^{-6}$  radians.

The cylinder exhibits a high-frequency vibration that varies in frequency and intensity with table speed. This vibration causes high-frequency waves on the water surface. Figure 4.4 shows the frequency spectra of these waves versus table speed. The vibration is minimal when the system turns without the platform, lucite plate, or tank mounted. It intensifies as each of these components is mounted; apparently the vibration increases as weight is added away from the table center. We placed a rectangular piece of lead between the bottom of the turntable and the laboratory bench in an attempt to minimize this vibration. We also isolated the entire rotating table assembly from extraneous laboratory vibrations by mounting it to a structural wall of the laboratory.

The table drive is provided by a DigiPlan Electronic Motion Control BL Brushless Servo Drive System. The system consists of a BL150 Drive with velocity feedback, a TO170 transformer, and an ML-3450, dc brushless motor. The signal travels from the computer to the drive, through the transformer where it is converted from 120V AC to 170V AC, back to the drive, and to the motor. The velocity feedback signal then comes back from the motor to the drive which corrects the velocity to ensure steady motion. This servo system broke down when the input voltage was greater than about 8 V (2.1 rad/s) at which point the rotation rate of the motor was unsteady. We note that prior to the acquisition of this motor we

Figure 4.4 Frequency Spectra of the Perturbative Surface Waves. (a) motor off, (b) motor on ( $\Omega_f = 0$ ),  $\Omega_f =$  (c) 0.26 rad/s, (d) 0.52 rad/s, (e) 0.65 rad/s, (f) 0.78 rad/s, (g) 1.04 rad/s, (h) 1.30 rad/s, (i) 1.56 rad/s, and (j) 1.82 rad/s. The ordinates are  $\ln(a)$ .



drove the rotating table with a stepper motor. Qualitatively, all of the results we report herein were present when we used the stepper motor, including the high-frequency vibration.

### 4.3 Flow Visualization

We visualized pathlines of the fluid using both a digital imaging and an analog video system. The first is a Kodak EktaPro EM Motion Analyzer, Model 1012. This system consists of a high-gain imager with a Nikon 35mm lens, a video processor, and a Sony Trinitron Color Video Monitor. The imager sensor has a 192 X 239 pixel array with 256 grey shades. The processor can store 1637 full frames of digital images in electronic memory at various rates from 50 to 1000 Hz. To obtain lower recording rates, and correspondingly longer time series, one must trigger the imager externally. We used a Tectronix TM502A signal generator to provide a 0-5V square pulse at frequencies between 15-50 Hz for this purpose. The processor has a reference reticule with built-in X-Y electronic crosshairs and a reference marker. We mounted the imager on a Bogen 3051 professional tripod. The imager views the rotating tank through a standard mirror mounted at about a 45° angle above the tank.

We used the EktaPro to track the location of the eddy centers as a function of time. (See §5.5) To this end, we used the reticule to determine the position of the center of the eddy. The errors inherent in this procedure are due to (1) the subjectivity of the observer, (2) the limited spatial resolution of the imager, and (3) the optical set-up of the imager/mirror system. By comparing the results obtained from two observers, we found that the errors due to (1) are small compared to those due to (2) and (3). The errors due to (2), which is the distance between pixels, introduce a standard deviation in position location of  $\pm 0.07$  in. To determine the errors due to (3), we tracked a mark on the tank bottom during rotation. Figure 4.5 displays the pathline we obtained. The error, which is a combination of error due to (2)

and (3), is  $\pm 0.25$  in. We transferred the images to VHS tapes using a Panasonic AG-1960 Multiplex VCR linked to the processor.

The analog video system was a Sony Hi-8 Video Camera Recorder, Model EVO-150TR. It records at 30 Hz directly onto tape. We mounted the camera directly above the rotating tank and used a remote controller for direct recording of the flow paths. We played the tapes on a Sony EVO-9800 VCR. To obtain "instantaneous" images of the flow, we photographed the monitor using a Nikon FM2 camera with a 50mm lens. These photographs are shown in §5.1 - 5.5. We found two problems associated with photographing the monitor. The first is that the monitor resolution limits the photograph resolution. The second is that the curvature of the monitor distorts the image. This distortion is especially apparent in Figures 5.5. It introduces errors of  $\pm 0.20$  inches into the measurements discussed in §5.6.

#### 4.4 The Rectangular Tank and Water

We constructed the  $11 \times 3\frac{2}{3}$  in<sup>2</sup> tank out of clear lucite, fastening the with a clear, fast-curing solvent cement. To vary the aspect ratio (length/width) from three to two, we used quarter- and half-inch inserts that fit tightly inside the box. The tank was filled with distilled water to the desired depth. The depth was measured using a Lory Type C point gauge accurate to 0.01 mm. Fluid motions were observed using red, green, and blue food coloring. A drop of the food coloring was applied to the surface and generally sank, creating a column through the water and a blob on the bottom. In most of the figures in §5, 3 drops were applied symmetrically along the two long sidewalls.

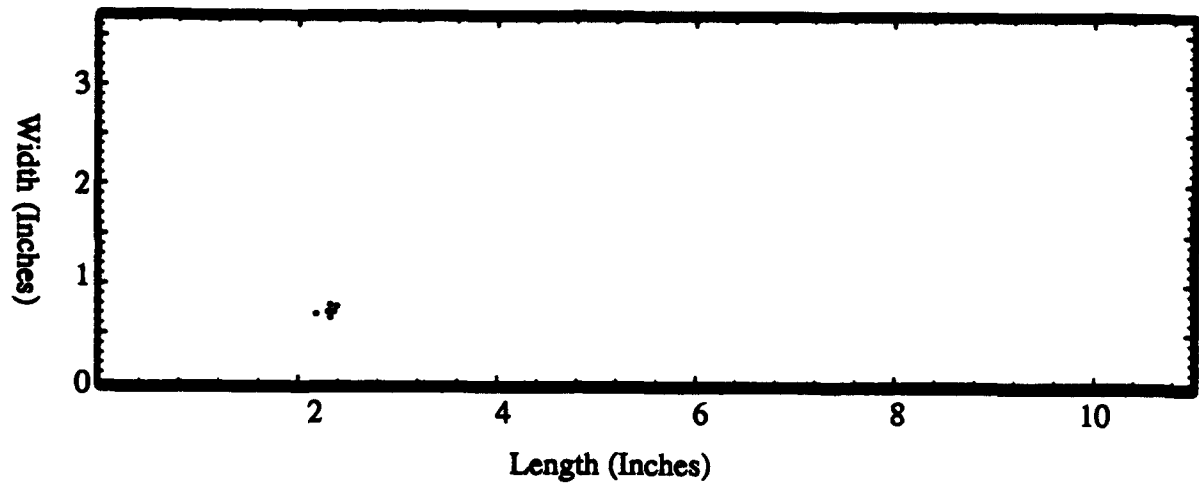


Figure 4.5 Data Points Showing Measurement Error for the Position of the Eddy Center

## Chapter 5

### RESULTS

In this chapter we present and discuss our observations of the pathlines of fluid that spins up in a rectangular cylinder when the rotation rate is impulsively changed from  $\Omega_0$  to  $\Omega_f$ . We begin by discussing a specific “comparison” case for which the horizontal aspect ratio of the cylinder,  $\delta = 3$ ,  $\Omega_0 = 0$ ,  $\Omega_f = 0.52$  rad/s, and the water depth,  $H = 5$  cm. This experiment is similar to one by vHDD, to which we compare our results. Next, we discuss qualitatively the effects of changing  $\delta$ ,  $\Omega_f$ , and  $H$ . Lastly, we show measurements of the path of an eddy center and a separation point in the flow. In all of these cases, we assess the flow as an observer in the inertial reference frame (not in the rotating frame) looking down on the tank. (We did several experiments in the rotating frame and our conclusions did not change.) Figure 5.1 is a schematic of the cylinder plan view; it shows what we will refer to as the “leading” corners, A and C, the “trailing” corners, B and D, the distances referred to as the “length” and “width” of the tank, and the angle  $\Theta$  that we refer to in §5.2.

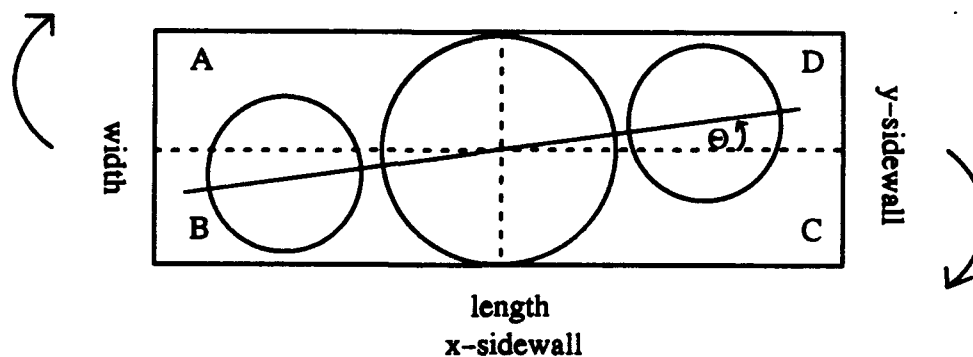


Figure 5.1 Plan View of the Rectangular Cylinder

### 5.1 Comparison Case

The series of photographs in Figure 5.2 show the pathlines of the flow for an experiment in which the fluid's angular velocity was changed from zero (initially it is at rest) to  $\Omega_f = 0.52$  rad/s (the final state is rigid body rotation) when  $\delta = 3$  and  $H = 5$ cm. We chose this experiment as a baseline for comparison with our other experiments and with an experiment performed by vHDD. In the following, we describe horizontal flow observations, vertical flow observations, and compare our results to the flow patterns of a similar experiment performed by vHDD.

#### *5.1a Horizontal Flow Observations*

When the tank began to spin, the fluid in the center of the tank was stationary. Fig 5.2a shows that within three seconds, a large anticyclonic flow developed that was similar to the initial flow described in §3.2 in the rotating reference frame. The fluid moved quickly along the x-sidewalls from D to A and B to C. In accordance with the no-slip boundary condition, the fluid on the wall stayed on the wall, so the edge of the anticyclonic cell provided some indication of the boundary layer thickness. Within 5–10 seconds, four cyclonic eddies formed in the corners of the tank. Figure 5.2b shows that the two cells in the leading corners were noticeably larger than those in the trailing corners. By about  $1 \frac{1}{3}$  rotations (Figure 5.2c) the leading corner cells grew while the trailing corner cells were no longer visible. Figure 5.2c also shows a separation point in the flow, with two small counter-rotating eddies on either side. This separation point remained a distinct feature of the flow; we show measurements of its path in §5.6. As the cyclonic cells grew, their centers moved out of the leading corners. We show measurements of such a path in §5.5. Figure 5.2d shows that the cyclonic cells divided the initial anticyclonic flow into a primary anticyclonic cell in the center of the tank, and two secondary anticyclonic cells in the trailing corners of the tank.

Figure 5.2 Photographs of Dyelines for Spin-up from Rest.  $T = 12.1$  s;  $\Omega_f = 0.52$  rad/s;  $\delta = 3$ ;  $L/H = 5.6$ ;  $E^{-1/2} = 36$ ; and  $t/T =$  (a) 0.25, (b) 0.76, (c) 1.36, (d) 1.88, (e) 2.04, and (f) 4.9.



(a)



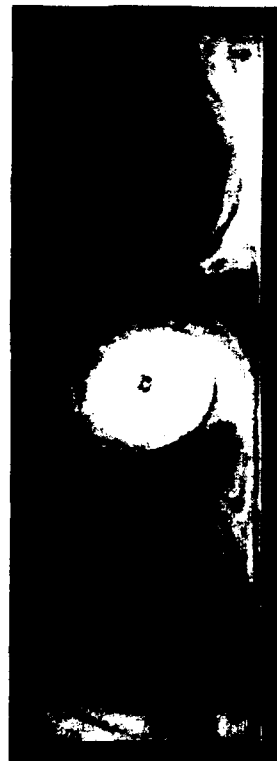
(b)



(c)



(d)



(e)



(f)

Figure 5.2e shows that by 2 rotations of the cylinder, the cyclonic cells spanned the width of the tank and the center anticyclonic cell was more nearly circular. A sharp edge was apparent between the two cyclonic and the center anticyclonic cells. The distinction was not so clear at the y-sidewalls of the box, where the secondary anticyclonic cells were still present. As the flow continued to spin up, the cyclonic cells continued to grow with their centers moving just past the y-centerline of the tank; the secondary anticyclonic cells occupied the entire y-sidewall with the prominent portion of the eddy now in the leading corners of the tank. Figure 5.2f shows the spun-up fluid. The pathlines formed an essentially 3-cell pattern, with the center anticyclonic cell flanked by two cyclonic cells. The center of the anticyclonic cell formed on the axis of rotation and remained there throughout spin-up. The size and position of the secondary anticyclonic cells after spin-up depended on  $\delta$ ,  $\Omega_f$ , and  $H$  as will be discussed in §5.2 – 5.5. The flow remained roughly antisymmetric about a horizontal diagonal of the cylinder throughout the spin-up process.

### *5.1b Vertical Flow Observations*

A definitive determination of the vertical flow was difficult to obtain for the experiments herein. Since the dye is heavier than the water, a slow sinking of dye was indistinguishable from a slow, secondary, downward flow. However, a secondary upward flow was unmistakable. From repeated observations, an approximate graph of the vertical flow in the primary eddies was obtained (See Figure 5.2.1). Figure 5.2.1a shows that the dyelines in the primary anticyclonic eddy spiraled up and into the interior of the eddy. The vertical coordinate increased like  $e^{\alpha\theta}$  where  $\alpha$  is  $O(0.1)$ , while the radial component decreased like  $Re^{-\beta\theta}$ , where  $R$  is the cell radius and  $\beta$  is  $O(0.01)$ . Vertical motion in the center of the anticyclonic eddy appeared to be downward. Figure 5.2.1b shows that dyelines in the two cyclonic eddies spiraled up and away from the center of the eddy. The vertical coordinate increased like  $e^{\alpha\theta}$ ,

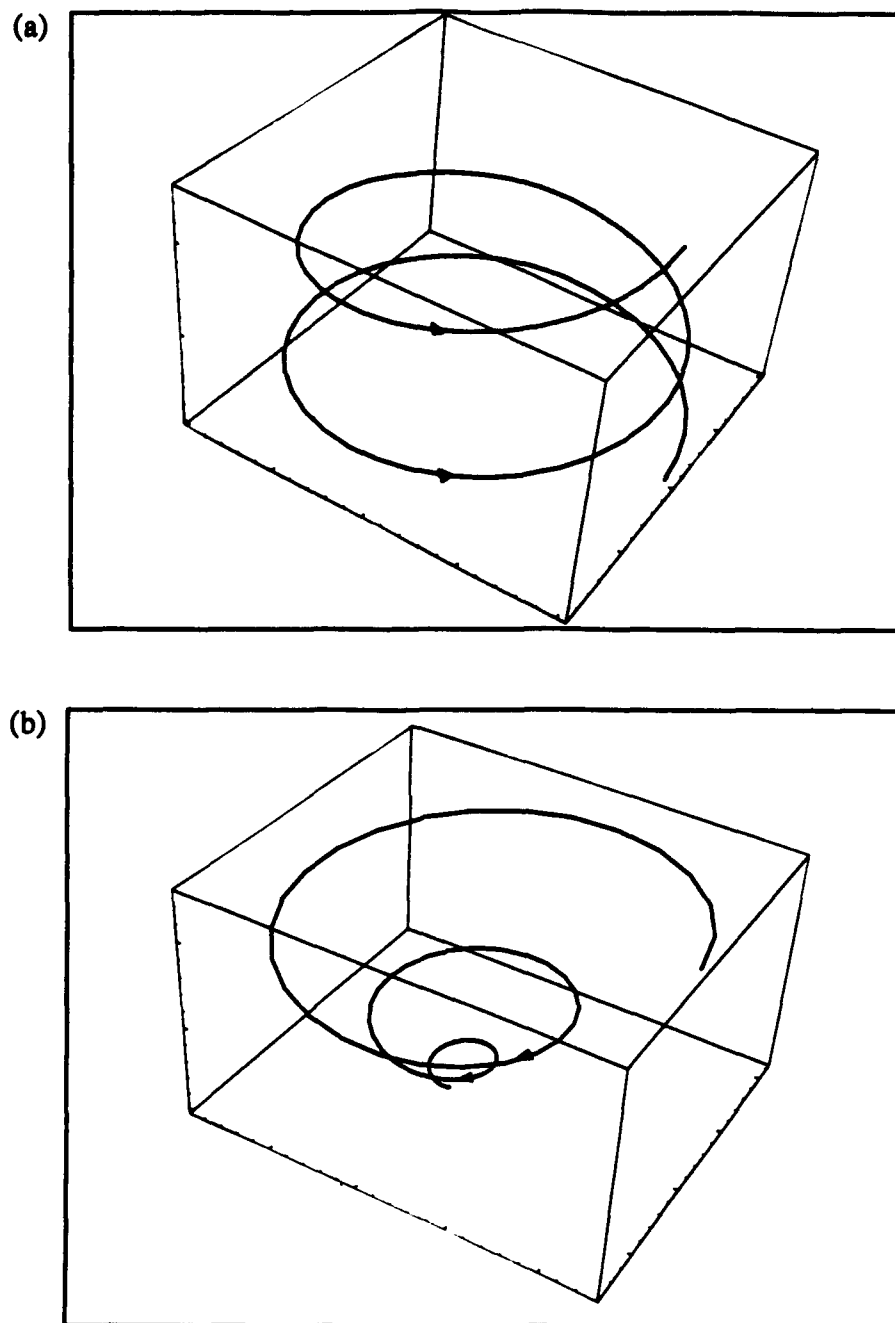


Figure 5.2.1 Approximate Trace for the Observed Vertical Flow Patterns in the Eddies. (a) anticyclonic, (b) cyclonic.

where  $\alpha$  is  $O(0.1)$ , while the radial component increased like  $Re^{\beta\theta} - R$ , where  $R$  is the eddy radius and  $\beta$  is  $O(0.1)$ . The vertical motion in the center of the cyclonic cells was upward.

### 5.1c Comparison with vHDD's Experiment

The flow described above differs fundamentally from the flow pattern of a similar experiment performed by vHDD. Table 1 shows the relevant parameters and non-dimensional numbers for the two experiments, which both had  $\delta = 3$  and  $\Omega_0 = 0$ . (We note that vHDD's fluid was either water or a dilute salt solution. It was not clear to the reader which is the case for this comparison experiment. The value of  $\nu$  given in Table 5.1 was obtained from calculations using given non-dimensional parameters.) The flow in their experiments began as in our comparison case with the initial anticyclonic cell and 2 cyclonic cells that grew out of the leading corners. vHDD, however, observed that the 2 cyclonic cells then divided the original anticyclonic cell into two anticyclonic cells which remained at the ends of the tank. The two cyclonic cells in the vHDD experiments moved toward the axis of rotation in the center of the tank where they merged into one cell. The pathlines to the final flow (rigid body rotation) consisted of three cells, a central cyclonic cell flanked by two anticyclonic cells. This final result is in complete contrast to our result of a central anticyclonic cell, flanked by two cyclonic cells.

We did observe an experiment in which the *final* result was similar to vHDD's; although, we cannot be sure that the evolution to this state was the same. In this experiment, which is discussed in detail in §5.4,  $\Omega_f = 1.82$  rad/s. The relevant parameters for this experiment are also shown in Table 5.1.

Table 5.1 Characteristic Parameters and Non-dimensional Numbers for One of vHDD's Experiments and Two Experiments Herein. The sense of the vorticity,  $\omega$ , in the 3 main cells formed by the pathlines of the flow is indicated as cyclonic (+) or anticyclonic (-).

Parameters	vHDD	Present Experiments	
		Comparison Case	Large $\Omega_f$ Case
$\text{sgn}(\omega)$	- + -	+ - +	- + -
$\Omega_f$	$0.57 \text{ s}^{-1}$	$0.52 \text{ s}^{-1}$	$1.82 \text{ s}^{-1}$
$\nu$	$0.005 \text{ cm}^2/\text{s}$	$.01 \text{ cm}^2/\text{s}$	$.01 \text{ cm}^2/\text{s}$
$L/H$	5.9	5.6	5.6
$E^{-1/2}$	160	36	65
$E_L^{-1/2}$	949	140	377
F	.1751	.0431	.5277

The most notable difference between the parameters for VHDD's experiment and that of the comparison case is in the difference between the Ekman numbers,  $E$ , of the two experiments. The magnitude of the Ekman number is affected by two main factors:  $H$  and  $\Omega_f$ . However, increases in  $E^{-1/2}$  due to increases in  $H$  *did not* affect the flow characteristics herein. For example, we conducted an experiment with  $\delta = 3$ ,  $\Omega_o = 0$ ,  $\Omega_f = 0.52 \text{ rad/s}$ , and  $H = 10 \text{ cm}$ . This experiment, for which  $E^{-1/2} = 72$ , showed the same flow characteristics as the comparison case. Increases in  $E^{-1/2}$  due to increases in  $\Omega_f$ , however, *did* affect flow characteristics. With each increase in  $\Omega_f$ , the 2 cyclonic vortices moved further toward the center of the tank (See §5.4 and 5.5). Eventually, when  $\Omega_f = 1.82 \text{ rad/s}$ , the cyclonic vortices joined and remained in the center of the tank. Based on this result, it appears that the - + -

vorticity pattern occurred when the cyclonic cells had enough energy to translate close enough to the center of the tank that they joined. We conjectured that if the box length was decreased, and the rotation rate is held constant, then the angular momentum of the corner cells would also decrease, and the cells may not have enough energy to translate to the center. Thus, it is likely that there are two scales important in this problem: the traditional Ekman number,  $E$ , based on depth, which defines the time scale required for spin-up (see §2) and an additional Ekman number,  $E_L = \nu/(\Omega_f L^2)$ , based on the box length, which provides some information on the evolution of the pathlines in route to spin-up. To test this idea further, we conducted an experiment in which  $\Omega_f = 1.82$  rad/s,  $\delta = 3$ , and  $L/H = 5.6$  (the same parameters which gave us a  $- + -$  vorticity pattern), but  $L$  was decreased to 8 inches. Here,  $E_L = 274$ , a value more comparable to the value of  $E_L$  for the comparison case. As anticipated, the dyelines in this experiment returned to the  $+ - +$  vorticity pattern of the comparison case. Thus, shortening the length of the cylinder decreased the tendency of the cyclonic cells to move into the center of the cylinder. Because the values of  $E_L$  for all of the experiments herein are actually about the same order of magnitude, further experiments are needed to determine more precisely if this scaling by cylinder length is an appropriate one.

Another possible explanation for the discrepancy between our experiments and those of vHDD is the difference in Froude number,  $F$ , between the experiments. Greenspan and Howard (1963) noted that the Froude number is a measure of the importance of free-surface effects relative to that of the Ekman layer. This difference does not seem to be a likely explanation as we conducted experiments with  $\Omega_f = 1.04$  and  $1.30$  rad/s, discussed in §5.4, having Froude numbers of 15.93 and 26.92, respectively, which did not display the same final result of a central cyclonic cell as vHDD's experiment did.

Another possible explanation is the presence of high-frequency waves on the surface of the water in the present experiments. vHDD attributed the translation of the cyclonic vortex toward the rotation axis to the parabolic shape of the undisturbed free upper surface of the fluid. It is possible that the high-frequency waves in the present experiments act as a perturbation of the free-surface that inhibits the cyclonic vortices from moving toward the center of the tank. To explore this possibility, consider the frequency spectra of the perturbative surface waves. The spectral data for the  $\Omega_f = 1.82$  rad/s shows a significant wave component at 144 Hz with only a small wave component at 19 Hz. This contrasts with the data for the comparison case,  $\Omega_f = 0.52$  rad/s, which had a number of small components across the frequency range. This difference in the spectra may support the conclusion that the surface waves affect the translation of the vortices. However, the frequency spectra for  $\Omega_f = 1.30$  and 1.56 rad/s is similar to the spectrum for  $\Omega_f = 1.82$  rad/s; yet, the dyelines for the  $\Omega_f = 1.30$  and 1.56 rad/s showed the same central anticyclonic vortex as the comparison case while the  $\Omega_f = 1.82$  rad/s dyelines showed a cyclonic vortex in the center.

### 5.2 Effects of Varying $\delta$

A series of experiments was conducted to determine the effect of decreasing the aspect ratio,  $\delta$ , from an approximately odd number, 3, to an approximately even number, 2. The first column of photographs in Figure 5.3 shows the dyelines after two rotations of the cylinder. Variations in the aspect ratio did not significantly affect the dyelines at this initial state of spin-up. The second column of photographs in Figure 5.3 shows the dyelines after spin-up. When  $\delta \geq 2.5$ , the results were similar to those in the comparison case in §5.1 above. The anticyclonic cells in the leading corners of the cylinder were very weak and each occupied only about 1/27th of the tank. The centers of the cyclonic cells moved just past the centerline of the cylinder toward the trailing corners, leaving the three main cells slightly

Figure 5.3 Photographs of Dyelines as a Function of  $\delta$ .  $T = 12.1s$ ;  $\Omega_0 = 0$ ;  $\Omega_f = 0.52 \text{ rad/s}$ ;  $L/H = 5.6$ ;  $B^{-1/2} = 36$ ;  
(a - g)  $t/T = 2$ ; (h)  $t/T = 10$ , (i)  $t/T = 11$ ; (j)  $t/T = 10$ ; (k)  $t/T = 11$ , (l)  $t/T = 9$ , (m)  $t/T = 9$ .





(a)



(b)



(c)



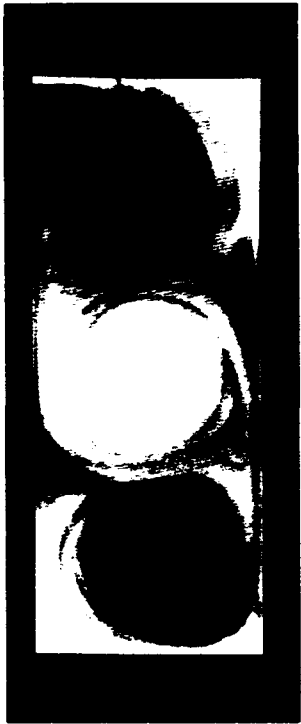
(d)



(h)



(i)



(j)



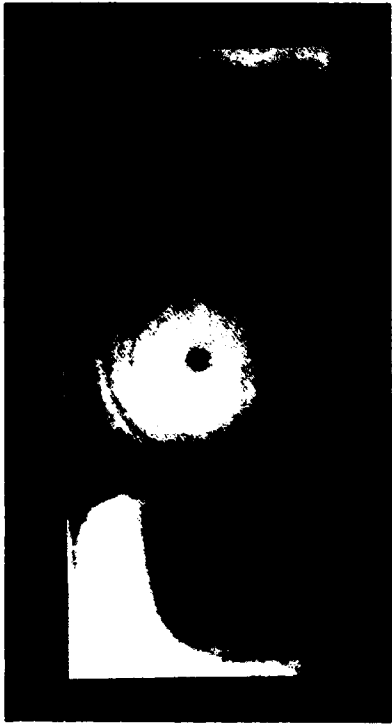
(k)

$\delta = 3$

$\delta = 2.75$

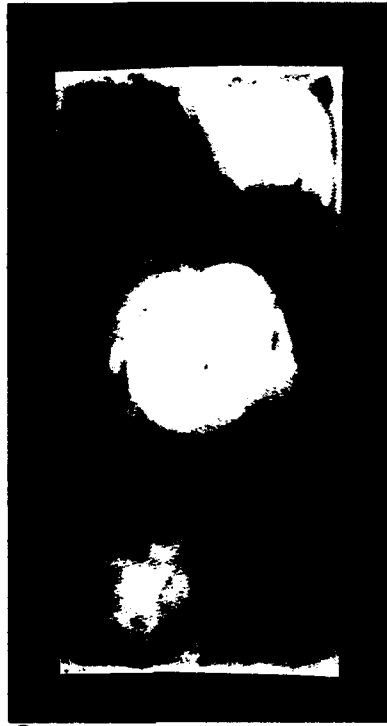
$\delta = 2.5$

$\delta = 2.38$



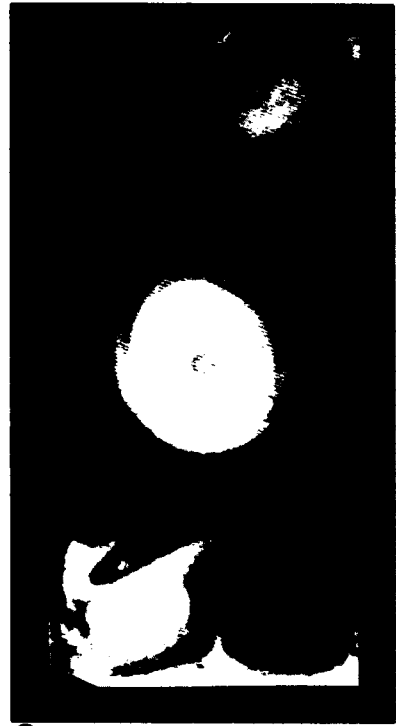
(l)

$\delta = 2.24$



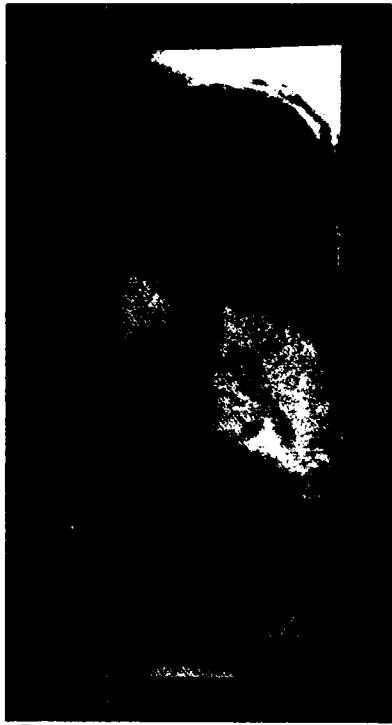
(m)

$\delta = 2.13$



(n)

$\delta = 2$



(e)



(f)



(g)

diagonalized. Figure 5.3h shows that when  $\delta = 2.38$  the secondary anticyclonic cells were slightly larger and began to entrain fluid from both the cyclonic cells and the primary anticyclonic cell. For  $\delta < 2.5$ , the initial state ( $t/T \cong 2$ ) was unchanged from when  $\delta \geq 2.5$ ; however, the final state was different. As  $\delta$  decreased from 2.38 to 2, the two secondary anticyclonic cells became more prominent and more off-center. A measure of the diagonalization of the three main cells is given by the angle,  $\Theta$ , between the line connecting the centers of the three main eddies and the y-centerline of the tank. Figure 5.4 shows that  $\Theta$  varied from  $2^\circ$  to  $30^\circ$  as  $\delta$  decreased from 3 to 2. When  $\delta = 2.24$ , each secondary anticyclonic cell was positioned in the leading corner of the tank and occupied about  $1/9$  of the tank once the fluid was spun-up. The cyclonic eddies still dominated, but  $\Theta$  was increased. When  $\delta = 2.13$ , each secondary anticyclonic cell grew to occupy about  $1/6$  of the tank at spin-up. The centers of the anticyclonic cells remained in the leading corners of the tank, while those of the cyclonic cells moved toward the trailing corners of the tank. Instead of having an essentially 3-cell pattern as resulted when  $\delta \geq 2.24$ , Figures 5.3m and 5.3n show that when  $\delta \leq 2.13$  the pattern consisted of essentially five cells with a large anticyclonic cell in the middle flanked by a cyclonic and a anticyclonic cell on each side. For all the experiments above, the flow remained roughly antisymmetric about a horizontal diagonal of the cylinder.

### 5.3 Effects of Varying $H$

Herein we discuss the results of experiments in which the depth,  $H$ , varied from 5 to 0.5 cm. The flow pattern was relatively unperturbed by depth variations except at the shallow depths of  $H \leq 1.0$  cm. In Figure 5.5 the first, second, and third columns show dyelines after 2, 4, and 6 revolutions, respectively. The fluid spun-up in all cases before 6 revolutions of the tank; when  $H = 1$  and 0.5 cm, the fluid spun-up before 4 revolutions. One consequence of decreasing depth was a corresponding decrease in the rotation rate of the cyclonic eddies.

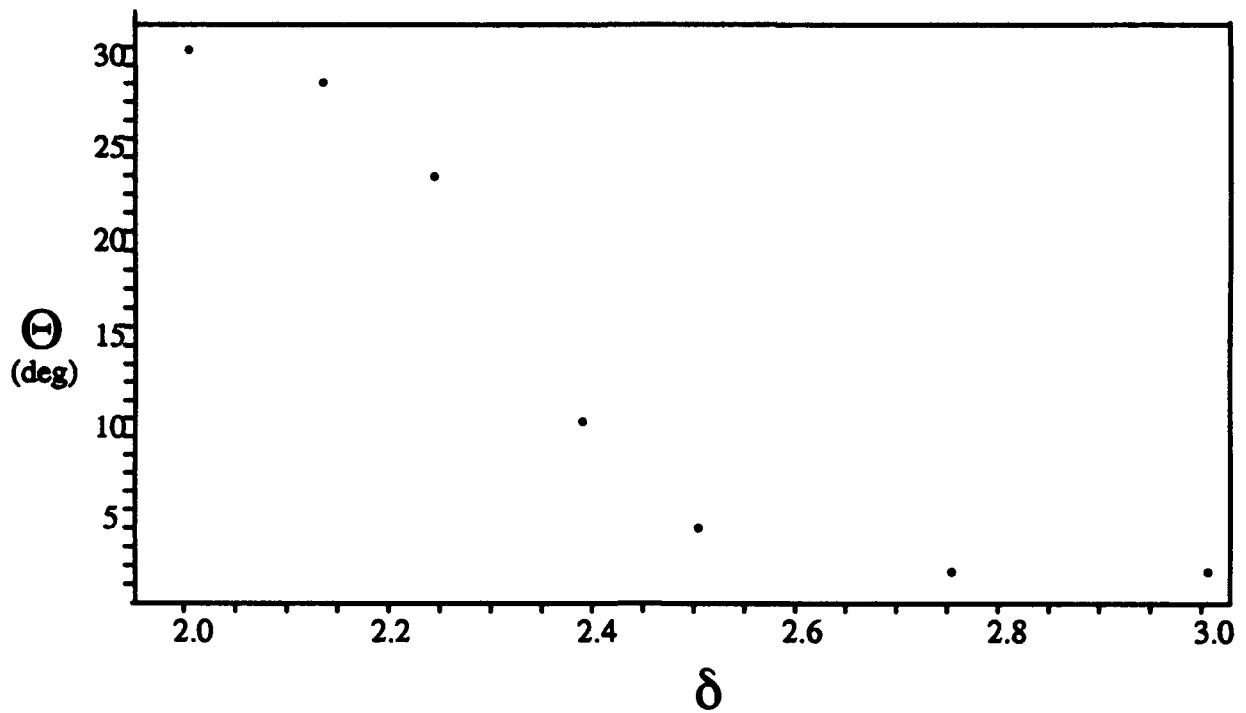


Figure 5.4 The Angle of the 3-Cell Axis as a Function of Aspect Ratio.  $T = 12.1\text{s}$ ;  $\Omega_0 = 0$ ;  $\Omega_f = 0.52\text{ rad/s}$ ;  $L/H = 5.6$ ;  $E^{-1/2} = 36$ .

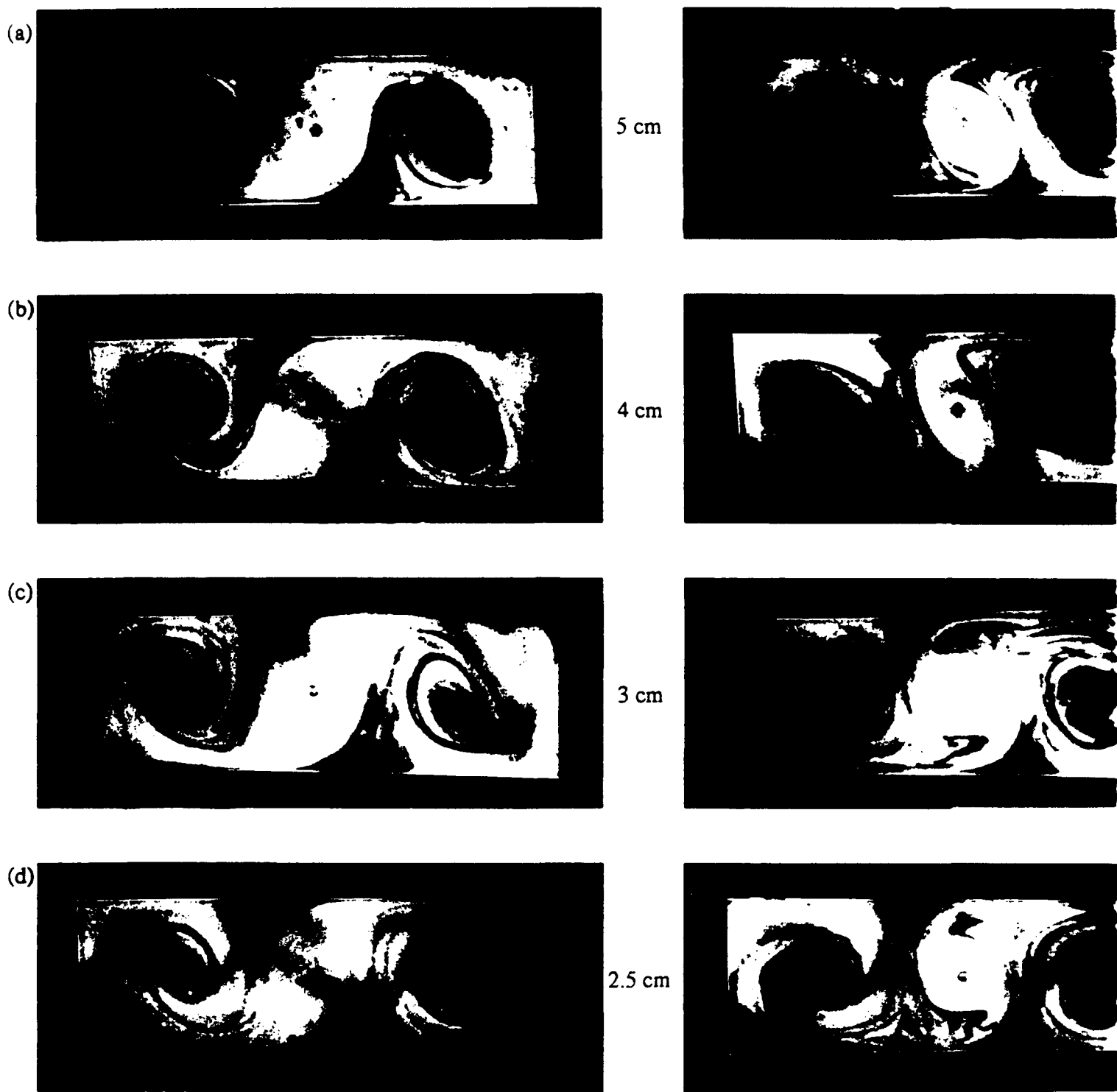


Figure 5.5 Photographs of Dyelines as a Function of Depth,  $H$ .  $T = 12.1$  s;  $\delta = 3$ ;  $\Omega_0 = 0$ ;  $\Omega_f = 0.52$  rad/s;  $t/T = 2$  (C)



5 cm



4 cm



3 cm



2.5 cm



;  $\Omega_f = 0.52$  rad/s;  $t/T = 2$  (Column 1),  $t/T = 4$  (Column 2),  $t/T = 6$  (Column 3); (cont on next page).

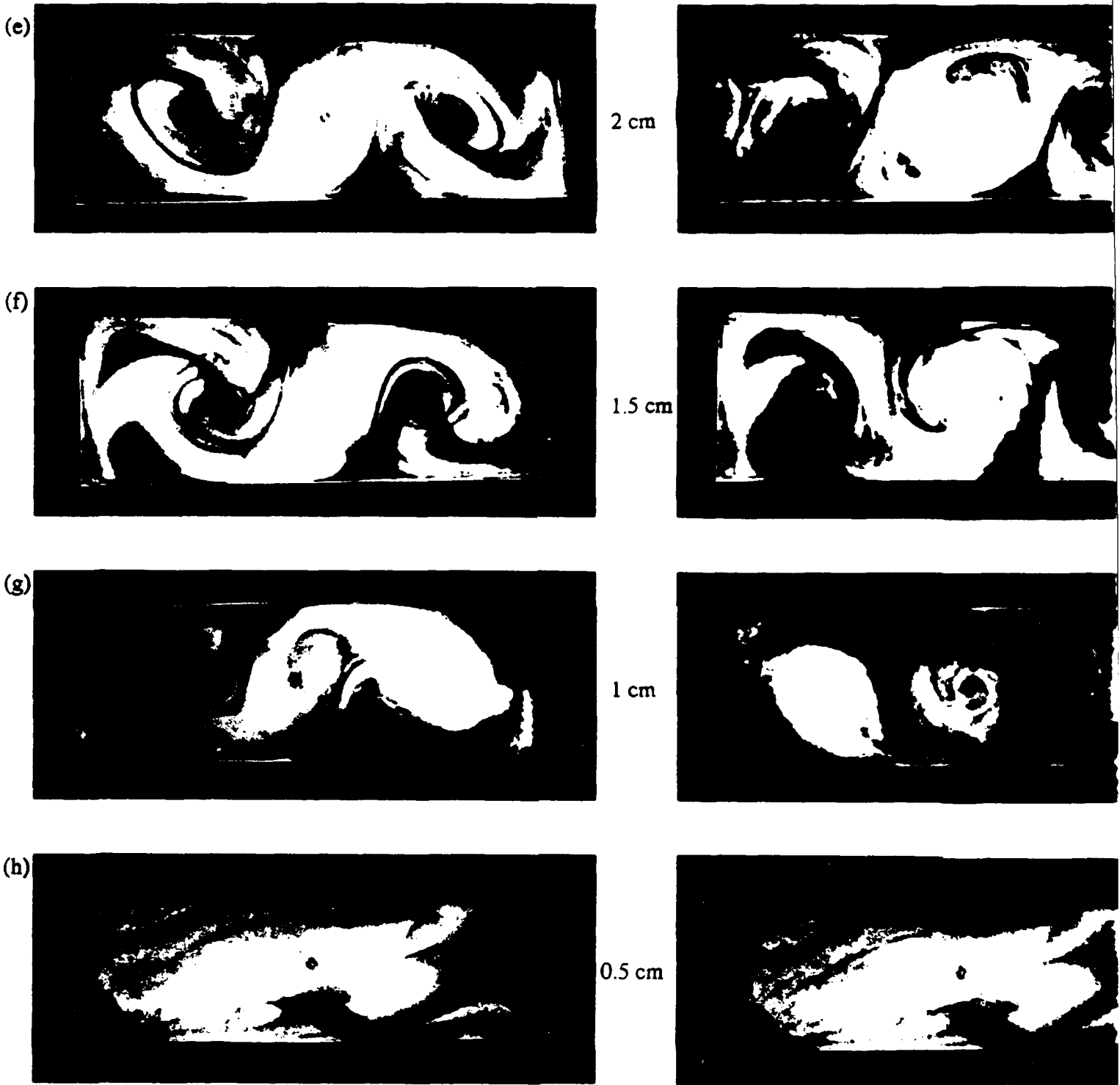


Figure 5.5 Cont.



2 cm



1.5 cm



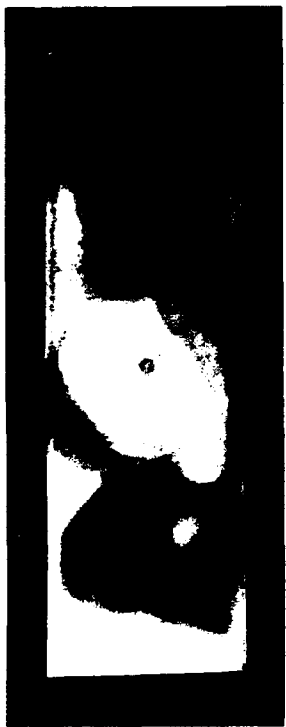
This decrease is evident in column 1 of Figure 5.5 as a lessening in the stretching and wrapping of the dyelines. Another consequence of decreasing depth was a corresponding decrease in the spin-up time. This conclusion is not obvious from Figure 5.5; see §5.7 for further discussion. Column 2 of Figure 5.3g shows that as a result of the decreasing flow speed and spin-up time, the shallow fluid ( $H \leq 1.0$  cm) spun-up before 3 closed circulation cells formed. This result was especially noticeable when  $H = 0.5$  cm. In that case, the fluid spun-up before the cyclonic cells moved into the tank. This decrease in spin-up time,  $T_E$ , is consistent with Greenspan and Howard's (1963) spin-up time scale,  $T_E \approx E^{-1/2} \Omega^{-1} = H/(\nu\Omega)^{1/2}$ , for fluid in a circular cylinder for which the secondary flow induced by the Ekman layer on the bottom boundary is the mechanism for spin-up (See §2).

We remark that the points of concentrated dye in Figure 5.5h are the original locations of the dye. The striations in the blue dye in column 2 of Figure 5.5h are the high-frequency waves discussed in §4.2. These waves became visible after spin-up when the dyelines were stationary and will be discussed in more detail in §5.6.

#### 5.4 Effects of Varying $\Omega_f$

In the experiments discussed here, the fluid spun-up from rest when  $\delta = 3$ ,  $H = 5$  cm, and  $\Omega_f$  was varied from 0.13 rad/s to 1.82 rad/s. Figure 5.6a shows that for the slowest rotation rate examined, the fluid behaved similarly to the shallow depth cases in that the cyclonic eddies moved away from the walls of the tank before they formed closed circulation cells. Column 2 of Figure 5.6a shows that the fluid spun-up before the center eddy closed off. A doubling of this rotation rate (Figure 5.6b) resulted in dyelines that were similar to those of the comparison case described in §5.1 and shown in Figure 5.6c. The dyelines at spin-up formed an essentially 3-cell pattern with two secondary anticyclonic cells in the

Figure 5.6 Photographs of Dyelines as a Function of  $\Omega_f$ .  $T = 12.1s$ ;  $\Omega_o = 0$ ;  $\delta = 3$ ;  $L/H = 5.6$ ;  $\psi T$  (Column 1) = 2,  $\psi T =$  (Column 2) = (a) 4, (b) 6, (c) 8, (d), 14, (e) 18, (f) 22, (g) 24, (h) 28.



$\Omega_f = 0.13$



$\Omega_f = 0.26$



$\Omega_f = 0.52$



$\Omega_f = 0.78$

(a)

(b)

(c)

(d)



$\Omega_f = 1.04$



$\Omega_f = 1.30$



$\Omega_f = 1.56$



$\Omega_f = 1.82$



(e)



(f)



(g)



(h)

leading corners of the cylinder. This pattern became more complex when the rotation rate was six times the slowest considered here. After spin-up (column 2 of Figure 5.6d), the dyelines were similar to those for the case of  $\delta = 2.24$ ,  $\Omega_0 = 0$ , and  $\Omega_f = 0.52$  rad/s described in §5.2 above; however, the evolution to this pattern was very complicated and not like that of the  $\delta = 2.24$  case. The flow began similarly with a central anticyclonic cell, which was quickly separated from the wall and deformed by the rapidly growing cyclonic cells formed in the leading corners of the cylinder. As the cyclonic cells moved away from the walls, anticyclonic cells were left at the end walls. These grew and wrapped into the cyclonic cells. At the same time, new cyclonic cells were forming in the leading corners of the cylinder. These secondary cyclonic cells also got pulled into the main cyclonic cells. This process continued as new cells formed in the corners, grew, and got pulled into the larger cyclonic cells. Column 2 of Figure 5.6d shows that fluid pathlines after spin-up formed an essentially 5-cell pattern -- a center anticyclonic cell flanked on each side by a dominant cyclonic cell and a secondary anticyclonic cell. The centers of the cyclonic cells were on the diagonal toward the trailing corners; the centers of the secondary anticyclonic cells were toward the leading corners. Figures 5.6e, f, and g show that the results for  $\Omega_f = 1.04$ , 1.30, and 1.56 rad/s, which are about ten times the slowest rate, were very similar to those just described. Column 1 of these figures shows that with each increase in  $\Omega_f$  the transient flow at the onset of spin-up became more turbulent. This turbulence was not evident after a few rotation periods as the dyelines became smooth. Column 2 shows the fluid pathlines at spin-up. The results most closely resembled those of vHDD, when  $\Omega_f = 1.82$  rad/s (see §5.1). For the large rotation rate, the dyelines at spin up formed an essentially 3-cell pattern. Unlike the results for slower speeds, and like the result of vHDD, the center cell was cyclonic and flanked by two anticyclonic cells. However, unlike the vHDD result, these cells were not

circular; the center cell was stretched out in an S-shape and the two anticyclonic cells were elongated on one side. The evolution to this circulation was very turbulent and complicated.

### 5.5 Path of the Eddy Center

We tracked the path of the center of one of the cyclonic cells formed at the corner for three different  $\Omega_f$ 's: 0.26, 0.52, and 1.04 rad/s ( $\delta = 3$ ,  $H = 5$  cm,  $\Omega_0 = 0$  for all cases). Figure 5.7 shows the measured paths. In all cases, the path of the center was a non-monotonic spiral to its endpoint with the center of the eddy ending up more toward the center of the cylinder than would be expected if the 3 cells equally divided the tank. The paths show that the eddy center was also off the y-centerline of the tank after spin-up. The centers of the cells ended at a location increasingly distant from the y-centerline as  $\Omega_f$  was increased. This conclusion is not obviously supported by the data for  $\Omega_f = 1.04$  rad/s in Figure 5.7 because the cell was not tracked all the way to spin-up, but the photographs in Figure 5.6 clearly support the conclusion. Figure 5.8 shows the distance of the eddy center from the corner of the cylinder as a function of time. As  $\Omega_f$  increased, the time required for the eddy center to move into the center of the tank decreased from  $t/T \approx 5$  to  $t/T \approx 2$ .

### 5.6 Path of a Separation Point of the Flow

We used photographs taken every two seconds as described in §4.3 to track the path of a separation point of the flow. The separation point formed along the long wall (and stayed on the wall) where the flow from the cyclonic eddy converged with the flow from the anticyclonic eddy, causing a portion of the fluid to move toward the wall where it separated into two small counter-rotating eddies as discussed in §5.1. Figure 5.9 shows the distance of the separation point along the x-endwall from the corner of the cylinder as a function of time. Once the tank began spinning, the separation point moved smoothly down the side of the

## Path of the Eddy Center

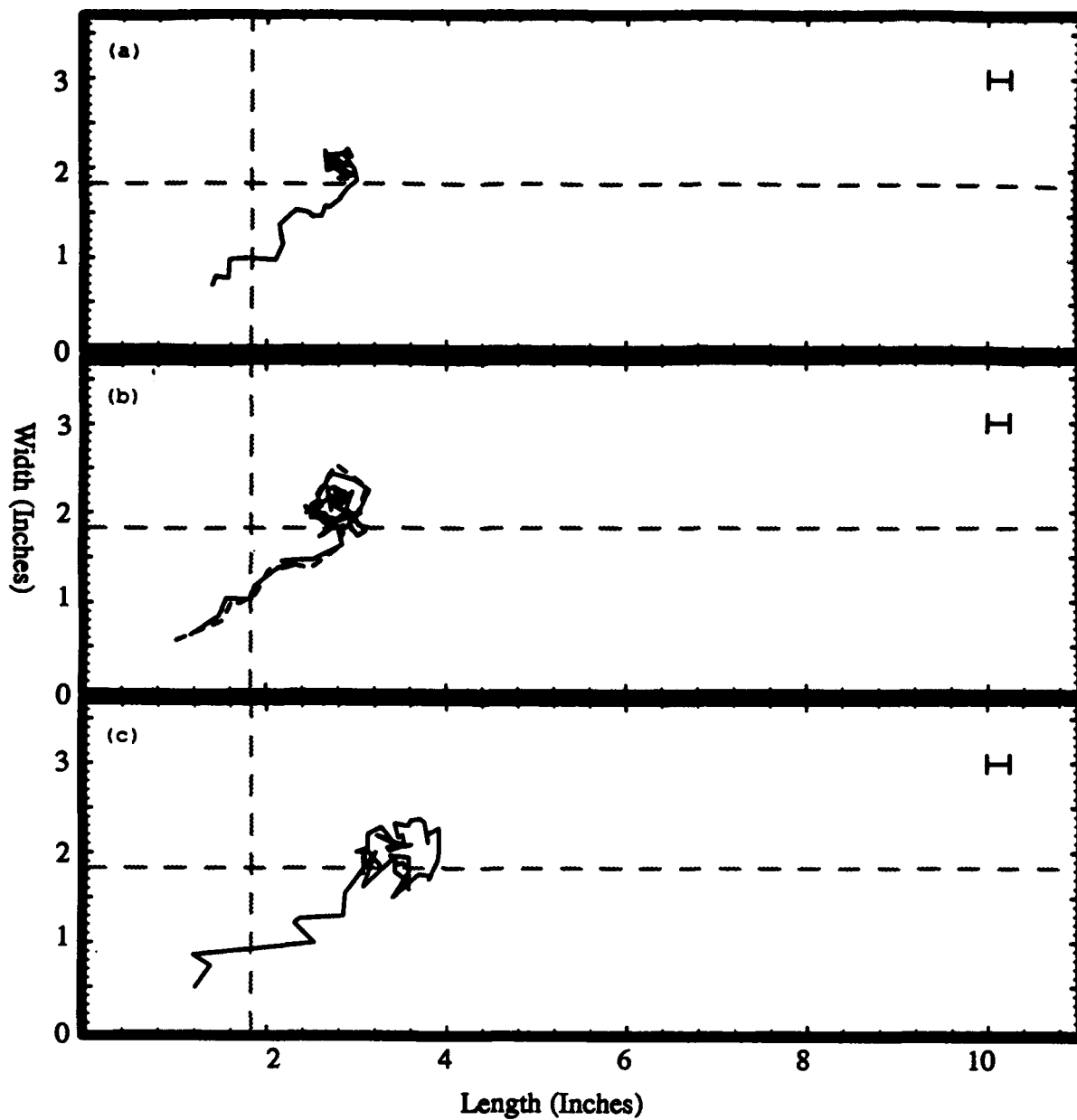


Figure 5.7 Path of the Center of the Cyclonic Eddy.  $H = 5$  cm;  $\Omega_0 = 0$ ;  $\delta = 3$ ;  $E^{-1/2} = 36$ ;  $\Omega_f =$  (a) 0.26, (b) 0.52; (—) Observer 1, (---) Observer 2, (c) 1.04 rad/s. The intersection of the  $x = L/6$  and  $y = W/2$  indicates where the center of the eddy would be if the 3 cells divided the tank equally. (The |—| shows the error of measurements.)

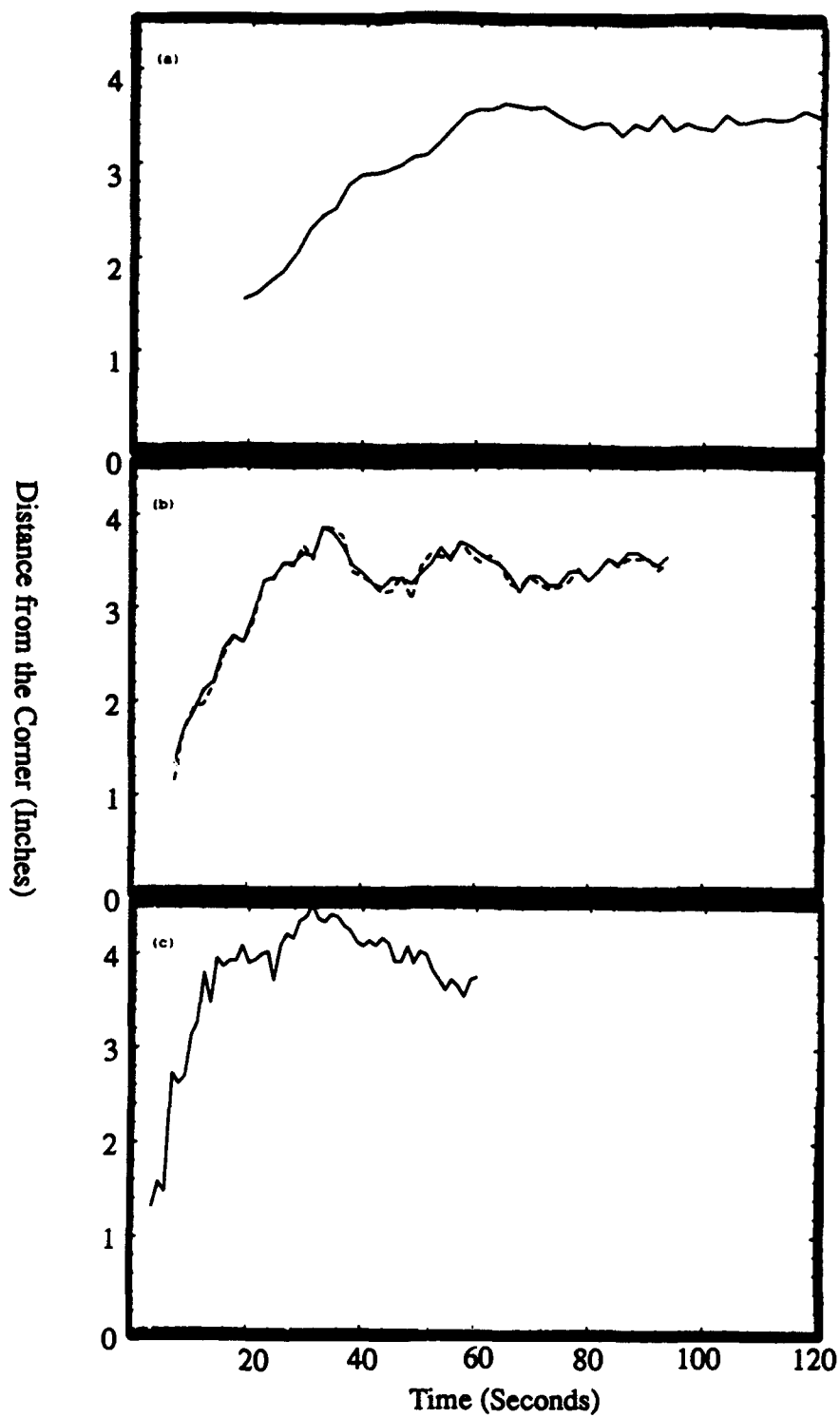


Figure 5.8 Distance from the Cylinder's Corner to the Center of the Cyclonic Eddy as a Function of Time.  $T = 12.1$  s;  $\Omega_0 = 0$ ;  $\delta = 3$ ;  $E^{-1/2} = 36$ ; and  $\Omega_f =$  (a) 0.26, (b) 0.52, ——— Observer 1, - - - - Observer 2, (c) 1.04 rad/s.

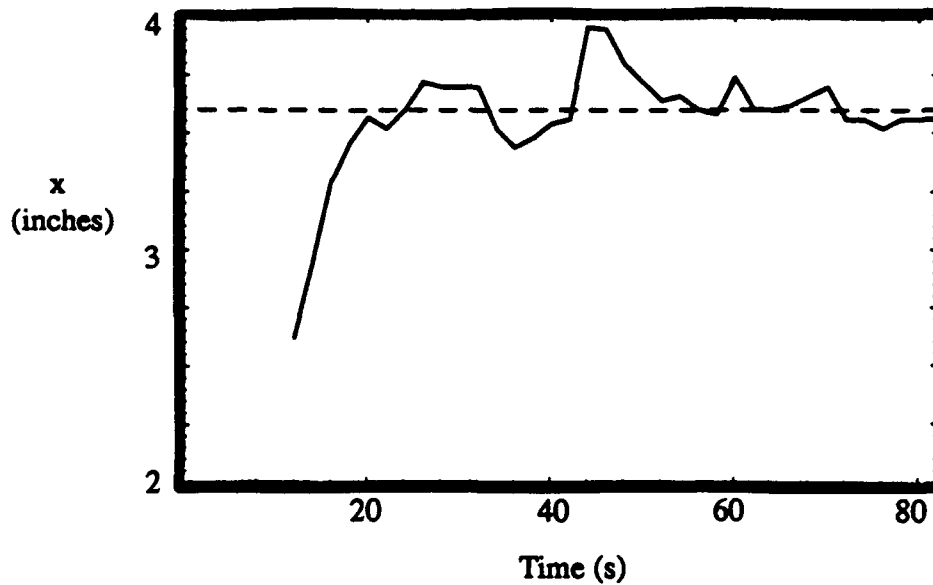


Figure 5.9 Path of a Separation Point of the Flow along the x-endwall.  $T = 12.1$  s;  $\Omega_0 = 0$ ;  $\delta = 3$ ;  $E^{-1/2} = 36$ ;  $L/H = 5.6$ ; and  $\Omega_f = 0.52$  rad/s. The dashed line indicates  $1/3$  of the distance along the wall.

cylinder. When it reached a position slightly less than  $1/3$  of the distance along the wall, it oscillated on the wall about that location.

### 5.7 Post Spin-up Phenomena

Several interesting flow patterns were observed at the latter stages of the spin-up process. We believe these phenomena occurred after the fluid achieved solid body rotation because they occurred several revolutions after visible changes in the dyelines were noted.

The first phenomenon observed was the striations in the fluid dyelines, which became visible after spin-up in the shallow depth cases as seen in Figure 5.10. These striations were predominantly seen toward the ends of the cylinder. They are evidence of the high-frequency surface waves discussed in §4.2



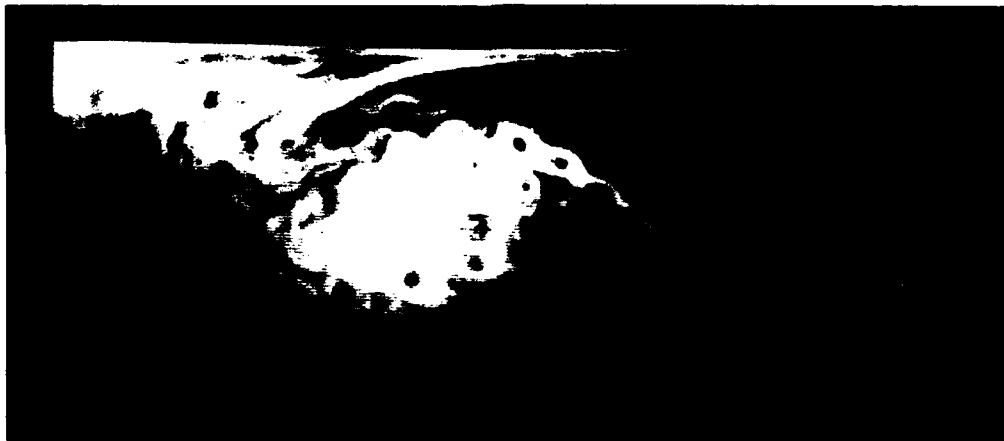
Figure 5.10 Surface Waves Evidenced in the Dyelines after Spin-up.  $T = 12.1\text{s}$ ;  $\Omega_0 = 0$ ;  $\Omega_f = 0.52\text{ rad/s}$ ;  $\delta = 3$ ;  $H = 1.0\text{ cm}$ ; and  $t/T = 6$ .



Figure 5.11 Post Spin-up Dyeline Instability.  $T = 12.1\text{s}$ ;  $\Omega_0 = 0$ ;  $\Omega_f = 0.52\text{ rad/s}$ ;  $\delta = 2.5$ ;  $H = 5.0\text{ cm}$ ; and  $t/T = 16$ .

The second phenomenon observed was the wavy pattern in the dyelines seen in Figure 5.11. This pattern was first discernable in the dyelines at the cylinder's center and later evident at the end walls. The third phenomenon noted was the small vortex formation as seen in Figures 5.12 and 5.13. These eddies formed first in the center of the cylinder and later spread throughout the fluid. Figure 5.13a shows a close-up of the eddies. The small counter-rotating eddies behind the large cyclonic cell are reminiscent of a Karman vortex street formed by flow past a cylinder at high Reynolds numbers. It is likely that the cause of the second and third phenomenon is the difference in surface tension and density of the water and the dye.

(a)



(b)

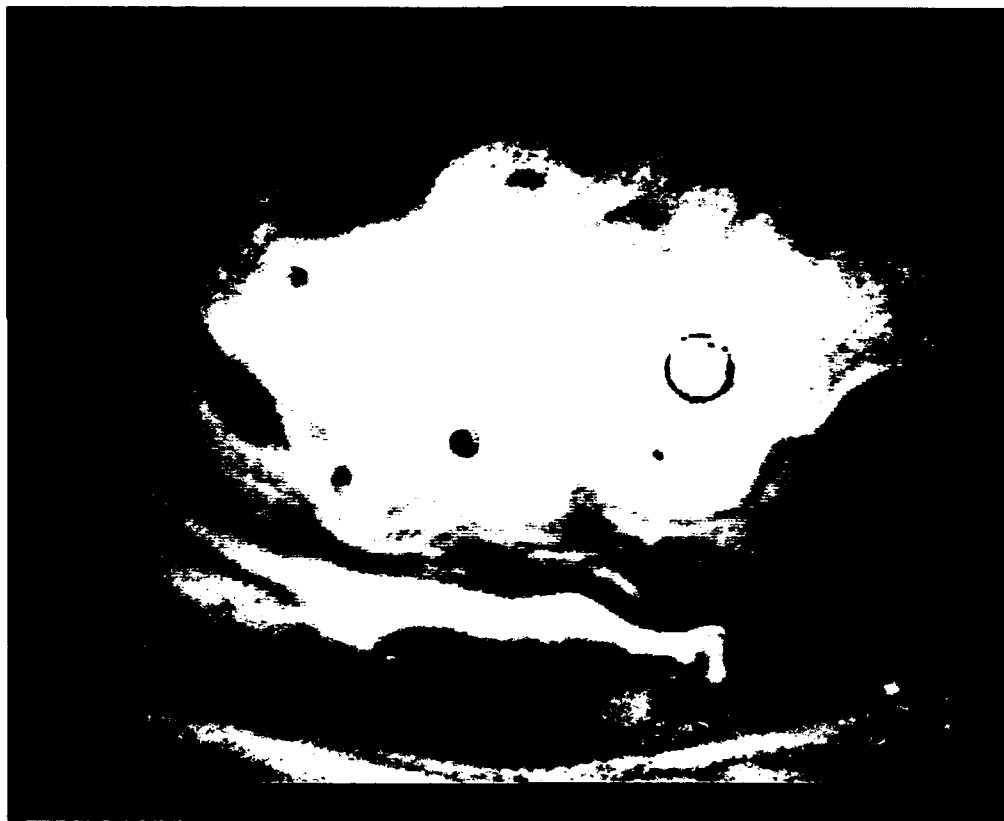


Figure 5.12 Post Spin-up Vortex Development.  $T = 3.0$  s;  $\Omega_0 = 0.78$  rad/s;  $\Omega_f = 2.07$  rad/s;  $\delta = 3$ ;  $H = 5.0$  cm; and  $t/T =$  (a) 58.25, (b) 52.25.

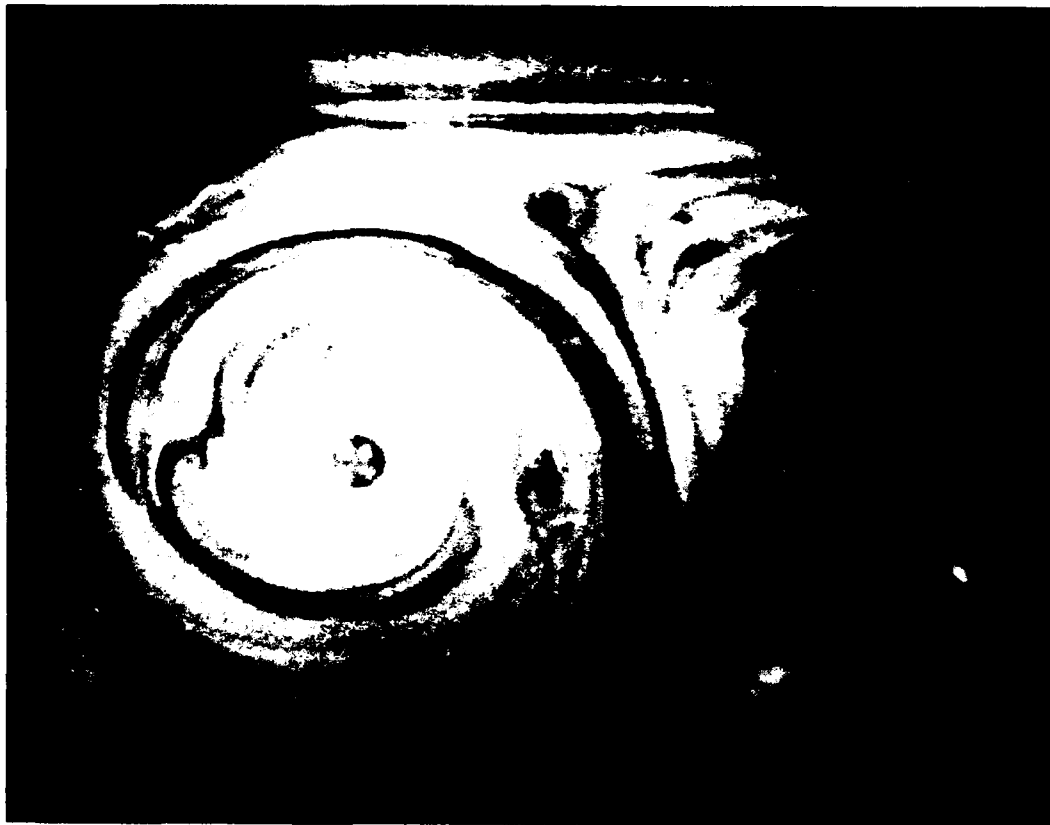


Figure 5.13 Post Spin-up Vortex Development.  $T = 12.1$  s;  $\Omega_0 = 0$ ;  $\Omega_f = 0.52$  rad/s;  $\delta = 3$ ;  $H = 2.0$  cm; and  $t/T = 9.75$ .

## Chapter 6

### CONCLUSIONS

The presence of corners in the rectangular cylinder caused the formation of eddies in the flow as the fluid was accelerated from rest to solid body rotation. The number of eddies, as well as eddy size, position, and rotation rate, were found to be dependent on  $\delta$ ,  $\Omega_f$ , and  $H$ . We evaluated our experiments against a comparison case for which  $\delta = 3$ ,  $\Omega_f = 0.52$  rad/s, and  $H = 5$  cm. Horizontal dyelines in this experiment formed a 3-cell, cyclonic-anticyclonic-cyclonic (- + -) pattern. The cells were near-circular. Small secondary anticyclonic eddies were observed in the trailing corners of the cylinder.

As  $\delta$  was decreased from 3 to 2, the size of the secondary anticyclonic cell increased. When  $\delta \leq 2.14$ , the flow evolved through 3 circular cells into an arrangement of 5 non-circular anticyclonic and cyclonic cells that were not aligned along a horizontal axis.

As  $H$  was decreased from 5 to 0.5 cm, a corresponding decrease in the spin-up time was observed. This confirmed the importance of the Ekman number,  $E = \nu/(\Omega_f H^2)$ , as a measure of the spin-up time scale. A decrease in the rotation rate of the cyclonic eddies was also observed as  $H$  was decreased.

As  $\Omega_f$  was increased from 0.13 to 1.82 rad/s, the centers of the cyclonic cells became more diagonalized and the tendency of the cyclonic cells to travel to the center of the cylinder increased. These tendencies were confirmed by the measurements of the cyclonic eddy paths discussed in §5.5. For a large enough  $\Omega_f$ , the cyclonic cells joined in the center of the cylinder, so that the final pathline of the flow was like that of vHDD. Comparison with the experiments of vHDD showed that the length of the cylinder, in addition to  $\Omega_f$ , was an important

factor affecting the tendency of the cyclonic eddies to move into the center of the tank. Thus  $E_L = \nu / (\Omega_f L^2)$  seems to be an important scale that is relevant to the evolution of the pathlines during the spin-up process.

Several interesting post spin-up phenomena, including dyeline instabilities and vortex development, were observed. It is likely that these instabilities are due to the differences in fluid properties, such as density and surface tension, of the dye and the water.

**BIBLIOGRAPHY**

- Benton, E.R. & Clark, A. 1974 *Ann. Rev. Fluid Mech.* **6**, 257-280.
- Greenspan, H.P. 1968 *The Theory of Rotating Fluids*. Cambridge University Press.
- Greenspan, H.P. & Howard, L.N. 1963 On a time dependent motion of a rotating fluid. *J Fluid Mech.* **17**, 385-404.
- Pond, S. & Pickard, G.L. 1983 *Introductory Dynamical Oceanography*. Pergamon Press.
- van Heijst, G.J.F. 1989 Spin-up phenomena in non-axisymmetric containers. *J Fluid Mech.* **206**, 171-191.
- van Heijst, G.J.F., Davies, P.A. & Davis, R.G. 1990 Spin-up in a rectangular container. *Phys. Fluids A* **2**, 150-159.
- Wedemeyer, E.H. 1964 The unsteady flow within a spinning cylinder. *J Fluid Mech.* **20**, 383-399.
- Weidman, P.D. 1976 On the spin-up and spin-down of a rotating fluid. Part 1. Extending the Wedemeyer model. *J Fluid Mech.* **77**, 685-708.
- Weidman, P.D. 1976 On the spin-up and spin-down of a rotating fluid. Part 2. Measurements and stability. *J Fluid Mech.* **77**, 709-736.